

The first observation of the M1 transition $\psi' \rightarrow \gamma\eta_c(2S)$

Hu Liu, Liangliang Wang*, Yaqian Wang, Ling Yu and Changzheng Yuan

March 29, 2011

Contents

1	Introduction	2
2	Samples	4
3	Event selection	4
4	Background study	8
4.1	Representation of mass spectrum	8
4.2	Backgrounds estimated by the inclusive MC sample	9
4.2.1	Background from $\psi' \rightarrow X + J/\psi, J/\psi \rightarrow l^+l^-$	11
4.2.2	Background from $K_S^0 K^\pm \pi^\mp (\gamma_{FSR})$	11
4.2.3	Background from $\pi^0 K_S^0 K^\pm \pi^\mp$	14
4.2.4	Background from continuum	16
4.2.5	Summary of the backgrounds for $\gamma K_S^0 K^\pm \pi^\mp$	17
5	Efficiency of the event selection and systematic uncertainties	17
5.1	Over all efficiency	17
5.2	Photon efficiency	17
5.3	Efficiency for K_S^0 reconstruction	22
5.4	Tracking efficiency for K, π from IP	22
5.5	Efficiency for χ^2 cut of kinematic fitting	22
6	Opening the mass box and the fitting of signal	24
7	Consistency checks	28
8	Results	30
9	Summary	33

*Email address: llwang@ihep.ac.cn

1 Introduction

Charmonia are bound states of a charm quark and a charm anti-quark by strong interactions, which are the lightest heavy quarks and very important to understand QCD theory at this energy region. In 1974, one member of this family J/ψ was first observed experimentally [1–3]. Subsequently, a series of charmonia were discovered and studied. Figure 1 shows the spectrum of the charmonia and the observed transitions among them. The heaviest charmonium resonance under $D\bar{D}$ mass is ψ' (3686.09 ± 0.04 MeV), which can decay radiatively into other lighter charmonia, such as $\psi' \rightarrow \gamma\eta_c(1S)$, $\psi' \rightarrow \gamma\chi_{cJ}$, ($J = 0, 1, 2$). But the radiative transition between ψ' and $\eta_c(2S)$ which is focused in this note was never observed before. The latest study on the transition $\psi' \rightarrow \gamma\eta_c(2S)$ was from CLEO-c, which didn't give strong evidence for this radiative decay [4]. According to PDG2010 [5], the most recent average of different measurements gives the mass of $\eta_c(2S)$ 3637 ± 4 MeV, width 14 ± 7 MeV. The production of $\eta_c(2S)$ was observed only in B meson decay and two-photon process. The only observed final states in the hadronic decay of $\eta_c(2S)$ is $K_S^0 K^\pm \pi^\mp$.

Considering recent status of the study of $\eta_c(2S)$, the observation of $\eta_c(2S)$ in ψ' radiative transition is still interesting, and the improvements on the measurements of the mass and width of $\eta_c(2S)$ are necessary to understand QCD theory at this energy region. And recently, BESIII collected $156.4 pb^{-1}$ of data at the energy of ψ' mass, corresponding to 106 ± 4 M ψ' events [6] which is already $7 \sim 8$ times of the statistics of BESII and ~ 4 times of CLEO-c. And the data quality is much better than BESII and at the same level as CLEO-c. So we have the better chance to observe the radiative transition between ψ' and $\eta_c(2S)$ with the largest ψ' data sample in the world so far.

The mass of $\eta_c(2S)$ is close to the one of ψ' , so the energy for the corresponding photon of this transition is about 50 MeV, which is a challenge to our experiment. Tagging of the final states of $\eta_c(2S)$ decay can really help to reduce the backgrounds for real transition photons, although the branching ratios are very small. And only $\eta_c(2S) \rightarrow K_S^0 K^\pm \pi^\mp$ and $\gamma\gamma$ were already observed in experiments, so the decay mode $\eta_c(2S) \rightarrow \gamma K_S^0 K^\pm \pi^\mp$ are chosen as the first try to search for $\eta_c(2S)$ in ψ' radiative transition at BESIII. But other decay modes will also be studied in the analysis series including $K^+ K^- \pi^0$, $2(\pi^+ \pi^-)$, $2(K^+ K^-)$, $\pi^+ \pi^- K^+ K^-$, $\pi^+ \pi^- p\bar{p}$, $3(\pi^+ \pi^-)$ and $K_S^0 K 3\pi$. The knowledge of $\eta_c(2S)$ and the branching ratio $\psi' \rightarrow \gamma\eta_c(2S)$, $\eta_c(2S) \rightarrow X$ (X is any of the exclusive decay modes to be studied) is still poor, and it is sure that we are searching for a small signal and don't want to be biased by the fluctuation of data (the number of events around $\eta_c(2S)$ is small¹). And we also know that at this moment, the full simulation is still in the stage of fine tuning and the difference between data and simulation can not be neglected. So it is really hard to believe the optimization of the event selection criteria with MC samples. So the event selection and analysis methods will be developed by looking related distributions of MC and data samples. The processes with the same final states $\psi' \rightarrow \gamma\chi_{cJ}$, $\chi_{cJ} \rightarrow X$ ($J = 1, 2$) will be taken as control samples to validate these selection and to check MC simulations. But all the work is done without looking at the mass spectrum for data around $\eta_c(2S)$ mass ($3.6 < M_{K_S^0 K \pi} < 3.66$ GeV) until all the backgrounds are well understood, which means that this work is a blind analysis.

¹Usually, the optimization of selection is performed by the maximizing of the figure of merit which is generally defined as $\frac{N_{signal}}{\sqrt{N_{data}}}$ (N_{signal} is the number of events for signal, N_{data} is the number of events for data), if the statistics of data is small, the optimization can be significantly affected by the the fluctuation of data, which will make the result biased.

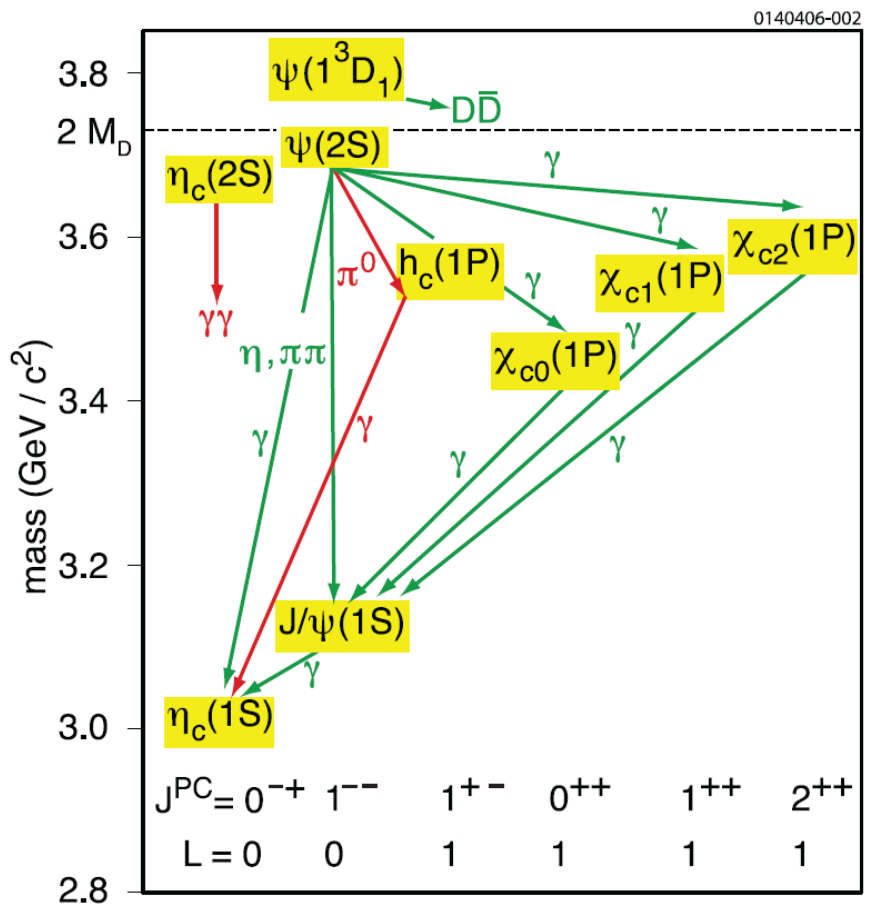


Figure 1: The spectrum of charmonia. The states are labeled with spectroscopic notation $n^{2S+1}L_J$, where n is the principal quantum number, S represents the spin of the particle and $S = 0, 1$, $L = S, P, D, \dots$ denotes the orbital angular momentum of $L = 0, 1, 2, \dots$, and J is the total angular momentum. In addition to this notation, parity (P) and charge conjugation (C) are used in the notation J^{PC} (for $c\bar{c}$ system, $P = (-1)^{L+1}$ and $C = (-1)^{L+S}$).

Table 1: Number of generated exclusive MC samples.

decay modes	number of events
$\psi' \rightarrow \gamma\eta_c(2S), \eta_c(2S) \rightarrow K_S^0 K\pi$	100000
$\psi' \rightarrow \gamma\chi_{c1}, \chi_{c1} \rightarrow K_S^0 K\pi$	100000
$\psi' \rightarrow \gamma\chi_{c2}, \chi_{c2} \rightarrow K_S^0 K\pi$	100000
$\psi' \rightarrow K^*(892)\bar{K}^0 + c.c \rightarrow K_S^0 K\pi$	100000
$\psi' \rightarrow \pi^+\pi^- K^+ K^-$	100000
$\psi' \rightarrow \pi^0 K_S^0 K\pi$	1000000

2 Samples

Besides $\sim 106M$ ψ' data collected by BESIII, 100M inclusive MC sample is generated, simulated and reconstructed just like real data to investigate the possible backgrounds(BG) from ψ' decay and another $42.6 pb^{-1}$ data set was collected at the energy 3.65GeV to estimate the BG from continuum contribution. And 1×10^5 MC events are generated for $\psi' \rightarrow \gamma\eta_c(2S), \eta_c(2S) \rightarrow K_S^0 K^\pm\pi^\mp$ to estimate the efficiencies for signal, where the mass and width of $\eta_c(2S)$ are set to 3637MeV and 14MeV respectively. Table 1 shows all the exclusive MC samples including reference channels and background channels used in the analysis, where K_S^0 is required to decay fully into $\pi^+\pi^-$.

The BESIII Offline Software System (BOSS) version used in the analysis is BOSS 6.5.1.p02 (Inclusive MC samples are produced by BOSS 6.5.1.²)

3 Event selection

In the selection of $\gamma K_S^0 K^\pm\pi^\mp$ events, $K_S^0 \rightarrow \pi^+\pi^-$ is used to tag K_S^0 . So firstly, the candidates are required to have 4 charged tracks with zero charge in total and at least one good photon.

Good photons should satisfy the following conditions: the reconstructed energy is larger than 25MeV , $0 \leq TDC \leq 14$, the direction should be in the active area of EMC ($|\cos\theta_y| < 0.8$ for the barrel part of EMC or $0.84 < |\cos\theta_y| < 0.92$ for the endcaps of EMC), and in order to reject the fake photons from the interactions between charged tracks and detectors, the angle between the position of the photon at EMC and the closest impact position of charged tracks at EMC should be larger than 20° .

To reconstruct K_S^0 , common vertex fit is performed for each charged track pair (4 possibilities in total in this case) in every event, where all the charged tracks are assumed to be pions. And the mother particles reconstructed from the previous fits are fitted to point to the interaction point (IP). The IP for each run is determined by averaging the event vertexes in each run, where event vertexes are obtained from the vertex fitting on the events with at least 3 charged tracks [7]. Only the charged track pair having an invariant mass in the window $|m_{\pi\pi} - m_{K_S^0}| < 15\text{ MeV}$ is regarded as the possible K_S^0 candidate in the event. If there are more than one candidates in the event, the one having the best fits (the smallest sum χ^2 of the vertex fit and the IP fit) is kept as the the K_S^0 candidate. In order to reduce the random combinations from events without K_S^0 , the decay length of K_S^0 candidate is asked to be larger than 0.5 cm (Figure 2). The invariant mass distributions for these K_S^0 candidates in data and inclusive MC sample are both shown in Figure 3, and finally only the events with K_S^0 candidate having the mass difference $|m_{\pi\pi} - m_{K_S^0}| < 7\text{ MeV}$, $\chi^2_{vtx} < 30$, $\chi^2_{IP} < 30$ are kept as good event candidates. The χ^2 distributions

²With BOSS 6.5.1, FSR photons are generated but not simulated. This bug is fixed in later BOSS release.

Table 2: The accuracy rates of the final states identification by $\chi^2_{K^\pm} + \chi^2_{\pi^\mp}$ only, χ^2_{4C} only and the total chi square (χ^2_{total}) for $\psi' \rightarrow \gamma\eta_c(2S) \rightarrow \gamma K_S^0 K^\pm \pi^\mp$ MC.

	$\chi^2_{K^\pm} + \chi^2_{\pi^\mp}$	χ^2_{4C}	χ^2_{total}
$K_S^0 K^+ \pi^-$	(95.92 \pm 0.18)%	(87.05 \pm 0.31)%	(97.16 \pm 0.15)%
$K_S^0 K^- \pi^+$	(95.88 \pm 0.18)%	(88.18 \pm 0.31)%	(96.89 \pm 0.16)%

for vertex fitting and IP fitting (primary vertex fitting) are shown in Figure 4. In order to reject $K_S^0 K_S^0$ backgrounds (e.g. $\psi' \rightarrow \gamma\chi_{cJ}, \chi_{cJ} \rightarrow K_S^0 K_S^0$ ($J = 0, 2$) see Figure 5), the other charge-opposite track pair in each event is required not satisfying the conditions of good K_S^0 candidates.

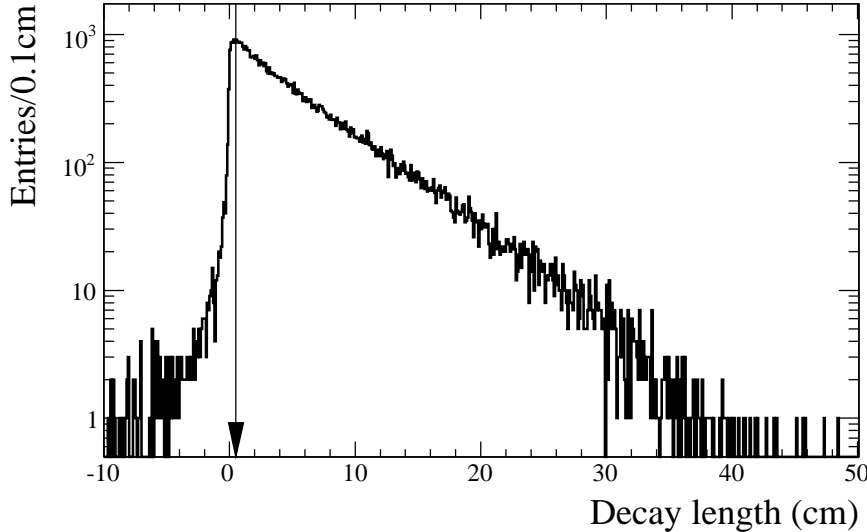


Figure 2: The decay length for the K_S^0 candidates in the $\psi' \rightarrow \gamma\eta_c(2S), \eta_c(2S) \rightarrow K_S^0 K^\pm \pi^\mp$ MC sample.

After the tagging of one K_S^0 by $K_S^0 \rightarrow \pi^+ \pi^-$, the other track pair of each event can be $K^+ \pi^-$ or $K^- \pi^+$. With these two assumptions, i.e. the two possible final states $\gamma K_S^0 K^+ \pi^-$ and $\gamma K_S^0 K^- \pi^+$, 4-constraints (4C) kinematic fits are performed for the final states of each event candidate, where the four constraints are the total energy and the three-dimensional momentum. If there are more than one good photons, all the photons are looped, and the best photon candidate is chosen by minimizing the chi-square of the 4C kinematic fit for either assumption. Then the chi-square of the 4C kinematic fit (χ^2_{4C}) and the chi-squares of the particle-identification for K ($\chi^2_{K^\pm}$) and π ($\chi^2_{\pi^\mp}$) are added together as the total chi square (χ^2_{total}) for each assumption, and Figure 6 shows χ^2_{total} with these two assumptions in a two-dimensional plane. As expected, the χ^2_{total} distribution peaks at small values with the right assumption, while with the wrong assumption, it becomes much wider. So the particle types of the other track pair are determined by choosing the smaller χ^2_{total} . In order to demonstrate the improvement of using the χ^2_{total} instead of χ^2_{4C} or $\chi^2_{K^\pm} + \chi^2_{\pi^\mp}$, the $\psi' \rightarrow \gamma\eta_c(2S) \rightarrow \gamma K_S^0 K^\pm \pi^\mp$ MC sample is used to test the accuracy rates of the final states identification which are shown in Table 2.

In order to give further rejection of the backgrounds having similar final states like $\pi^0(\gamma\gamma)K_S^0 K\pi$,

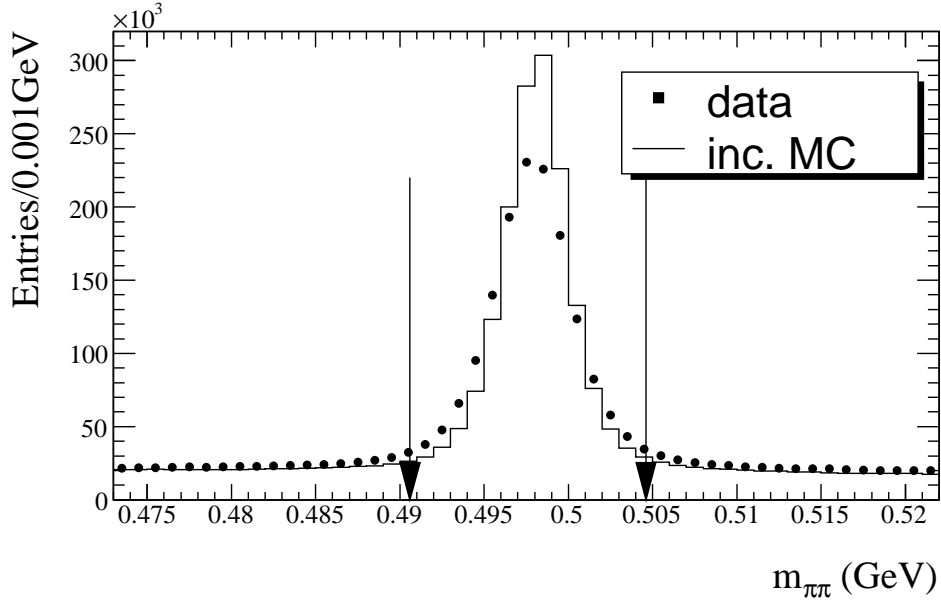


Figure 3: The invariant mass of the pion pairs which are selected as K_S^0 candidates.

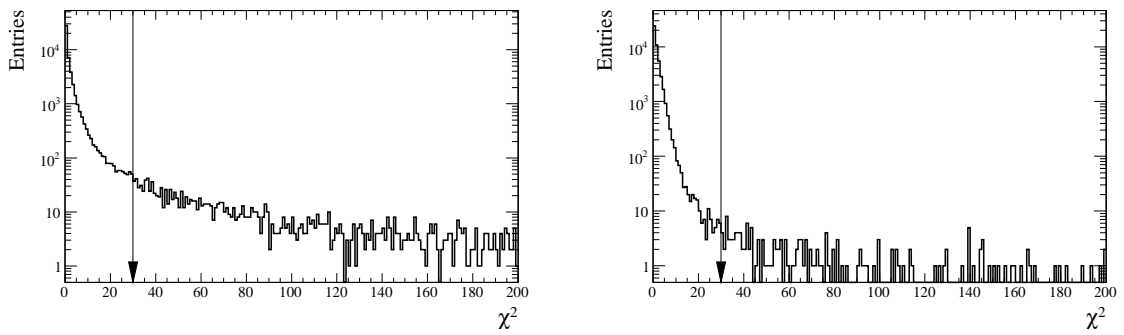


Figure 4: The χ^2 distributions for the secondary vertex fitting (left) and primary vertex fitting (right) of the K_S^0 candidates in the $\psi' \rightarrow \gamma\eta_c(2S), \eta_c(2S) \rightarrow K_S^0 K^\pm \pi^\mp$ MC sample.

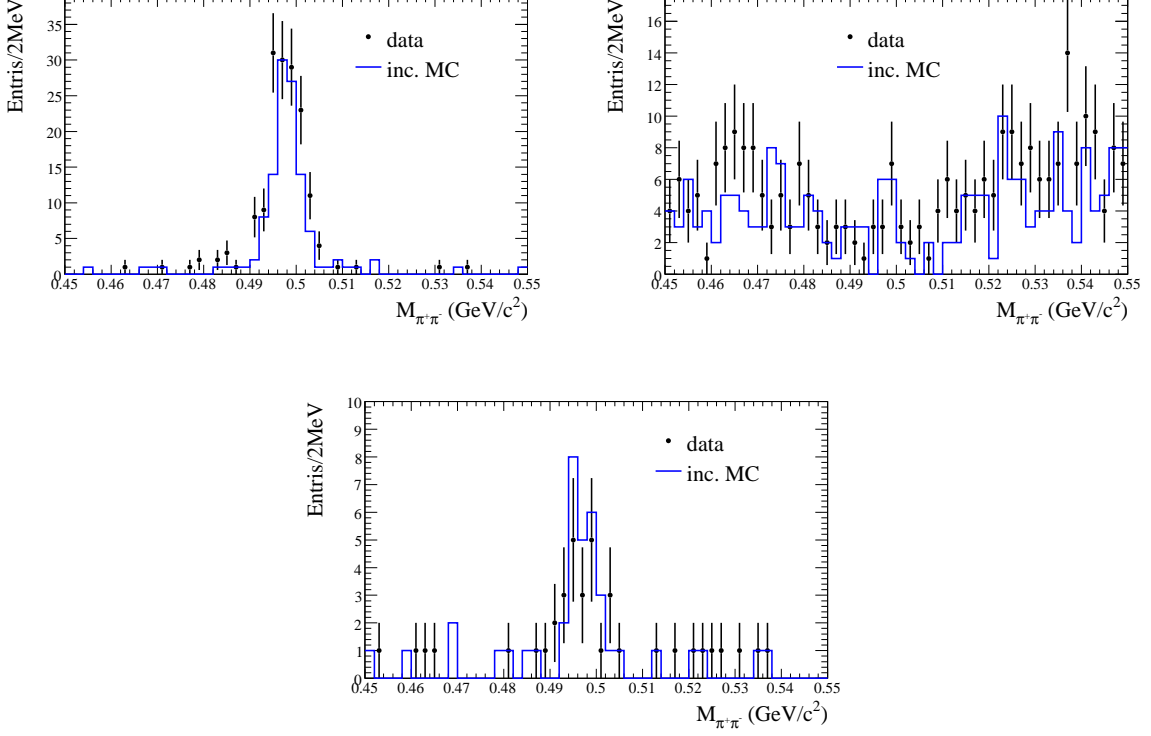


Figure 5: The invariant mass of the other track pair which are assumed as $\pi^+\pi^-$ for χ_{c0} (top left), χ_{c1} (top right) and χ_{c2} (bottom) by requiring $M_{K_S^0 K^\pm \pi^\mp}^{3C} \in [3.4, 3.46]\text{GeV}/c^2$, $M_{K_S^0 K^\pm \pi^\mp}^{3C} \in [3.49, 3.53]\text{GeV}/c^2$ and $M_{K_S^0 K^\pm \pi^\mp}^{3C} \in [3.54, 3.58]\text{GeV}/c^2$ respectively.

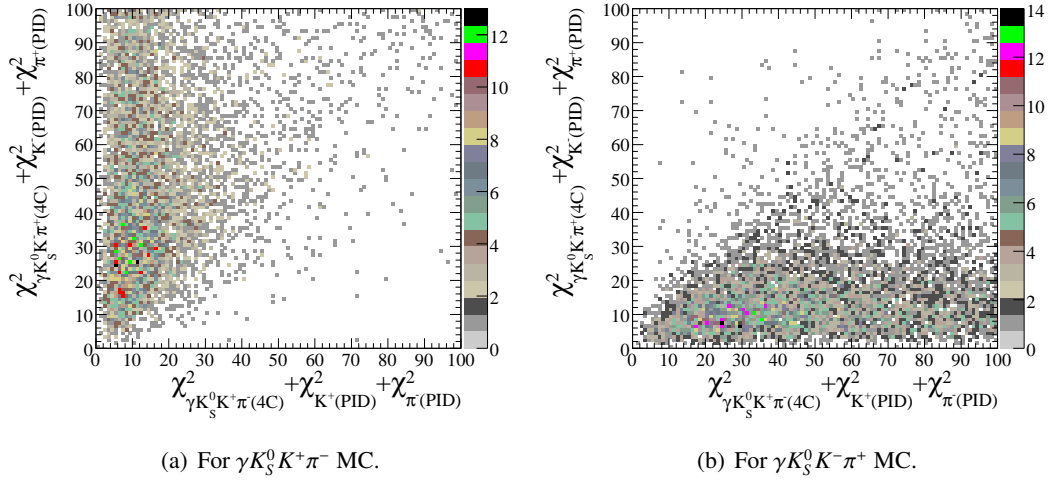


Figure 6: The χ^2_{total} distribution with $\gamma K_S^0 K^+ \pi^-$ assumption versus the one with $\gamma K_S^0 K^- \pi^+$ assumption.

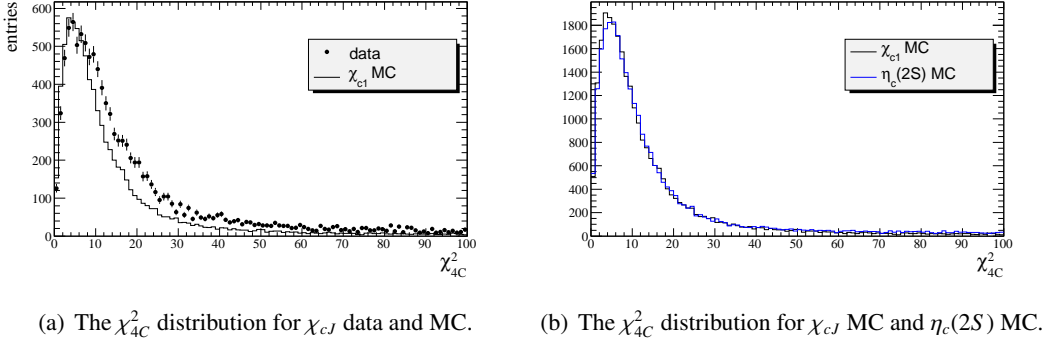


Figure 7: The χ^2_{4C} distributions for $\gamma K_S^0 K^\pm \pi^\mp$ events.

$K_S^0 K\pi$, $\gamma\pi^+\pi^-K^+K^-$ and so on, one has to require the 4C kinematic fits are reasonably good. The χ^2_{4C} distribution for data is wider than MC as shown in Figure 7(a), where both distributions are taken from $\psi' \rightarrow \gamma\chi_{cJ}, \chi_{cJ} \rightarrow K_S^0 K\pi$ candidates by asking mass $M_{K_S^0 K\pi}^{3C}$ between 3.47GeV and 3.60GeV (the mass $M_{K_S^0 K\pi}^{3C}$ will be defined in Section 4.1). The χ^2_{4C} distributions for $\psi' \rightarrow \gamma\eta_c(2S), \eta_c(2S) \rightarrow K_S^0 K\pi$ MC and χ_{cJ} MC are compared in Figure 7(b). The χ^2_{4C} distribution is slightly wider for $\eta_c(2S)$ MC than χ_{c1} MC, but they are still consistent with each other in first order. So the χ^2_{4C} distribution for χ_{cJ} data can be taken as a good prediction for $\eta_c(2S)$. And according to the distribution for data, the χ^2_{4C} is required to be less than 50.

4 Background study

4.1 Representation of mass spectrum

Before the detailed background study, the mass spectrum should be defined clearly. The invariant mass of $K_S^0 K^\pm \pi^\mp$ can be calculated from the reconstructed charged tracks or from the measured energy of the best photon candidate or from the 4C kinematic fit, and they are all shown in Figure 8(a) by taking $\psi' \rightarrow \gamma\eta_c(2S), \eta_c(2S) \rightarrow K_S^0 K^\pm \pi^\mp$ MC for instance. Obviously, the reconstructed mass has a systematic mass shift compared to the input $\eta_c(2S)$ mass ($3.637\text{GeV}/c^2$) and has the worst resolution among these masses shown here. The mass from 4C kinematic fits has the best resolution, and the mass from the measured energy of the best photon candidate is very close to it. But the effects near $3.66\text{GeV}/c^2$ are observed in both the 4C mass and the mass from the measured energy of the best photon, which are caused by the energy cutoff at 25MeV for the measured photons. According to the studies in the following section, one of the remained main backgrounds for $\psi' \rightarrow \gamma\eta_c(2S), \eta_c(2S) \rightarrow K_S^0 K^\pm \pi^\mp$ is $\psi' \rightarrow K_S^0 K^\pm \pi^\mp$ which contaminate the signal events mainly through fake photons. If the 4C mass is used to show the mass spectrum, the background from $\psi' \rightarrow K_S^0 K^\pm \pi^\mp$ will lie in $\eta_c(2S)$ mass region by a upward slope which peaks around $3.66\text{GeV}/c^2$ and decreases very sharply due to 25MeV energy threshold for photons (the black histogram in Figure 8(b)). As already mentioned, most of the $K_S^0 K^\pm \pi^\mp$ events survive because of fake photons, which means that the information of the best photon candidate used in the 4C fitting for these background events is not true, which bias the mass from 4C kinematic fit. In order to reduce the bias but still keep the resolution close to the best case (4C mass), a method is found to represent the mass spectrum — 3C kinematic fit, where the measured energy of the best photo

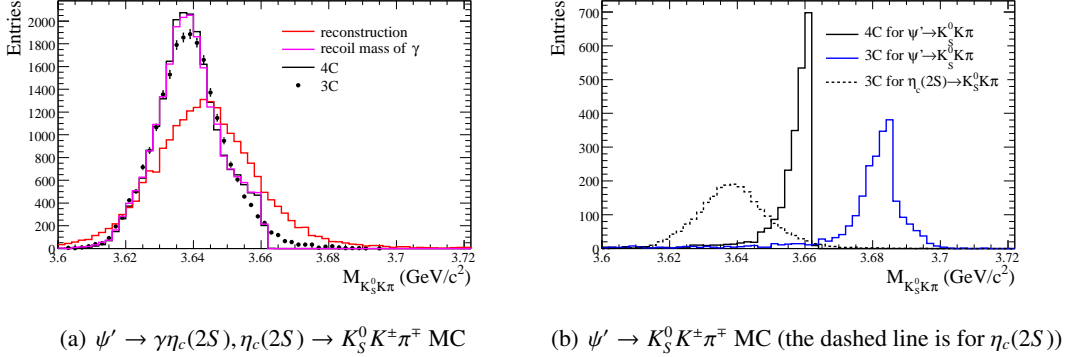


Figure 8: The $M_{K_S^0 K^\pm \pi^\mp}$ distributions obtained from different methods.

candidate is not used as an input to the fitting, i.e., the energy of the photon is allowed to be floating in the 3C kinematic fit. In this way, as the energy for fake photons prefers to float to zero, most of the background from $\psi' \rightarrow K_S^0 K^\pm \pi^\mp$ with fake photons will be pushed away and lie around ψ' mass as shown in Figure 8(b), which means that, in this mass region where the photon is soft, the 3C mass can make a better separation of background and signal in the mass spectrum. While the resolution for 3C mass is still at the same level as 4C mass as shown in Figure 8(a).

As a summary, 4C kinematic fit is still used to select events, because of better power of background rejection. While after selection, 3C kinematic fit is used to calculate the mass because of better separation of background and signal on the mass spectrum, and good resolution which is close to the 4C mass.

4.2 Backgrounds estimated by the inclusive MC sample

In this analysis, only the backgrounds with $M_{K_S^0 K\pi}$ around $\eta_c(2S)$ mass are crucial. But the processes $\psi' \rightarrow \gamma \chi_{cJ}, \chi_{cJ} \rightarrow K_S^0 K\pi (J = 1, 2)$ contribute exactly the same final state events and the $M_{K_S^0 K\pi}$ of which gives two big peaks just below $\eta_c(2S)$ mass. As already mentioned, these two clear signals from the radiative transitions between ψ' and $\chi_{cJ} (J = 1, 2)$ will be taken as the reference channels. So the backgrounds in a larger mass range $3.47 \text{ GeV} < M_{K_S^0 K\pi} < 3.7 \text{ GeV}$ will be investigated. For convenience, the mass range $3.47 \text{ GeV} < M_{K_S^0 K\pi} < 3.6 \text{ GeV}$ will be called χ_{cJ} mass region and the mass range $3.6 \text{ GeV}/c^2 < M_{K_S^0 K\pi} < 3.66 \text{ GeV}/c^2$ will be called $\eta_c(2S)$ mass region (i.e. signal mass region).

According to the inclusive MC sample, the main backgrounds in $\eta_c(2S)$ mass region are $\psi' \rightarrow X + J/\psi, J/\psi \rightarrow l^+ l^-$ (e.g. $\pi^+ \pi^- J/\psi, \eta J/\psi$ with $\eta \rightarrow \pi^+ \pi^- \pi^0 \dots$) and $K_S^0 K^\pm \pi^\mp \gamma_{FSR}$ (FSR: final state radiation). In χ_{cJ} mass region the main background is $\pi^0 K_S^0 K^\pm \pi^\mp$ which has little effect in $\eta_c(2S)$ mass region (only two events predicted by the inclusive MC sample).

With all the event selection requirements (including J/ψ veto described in Section 4.2.1), the mass spectrum of the remained backgrounds estimated by inclusive MC sample is shown in Figure 9 and the corresponding topologies of these backgrounds are listed in Table 3. The backgrounds in the signal mass region ($3.6 < M_{K_S^0 K^\pm \pi^\mp}^{3C} < 3.66 \text{ GeV}/c^2$) is quite few, except the radiation events ($K_S^0 K^\pm \pi^\mp (\gamma_{FSR} \text{ or } ISR)$) which are not included in the inclusive MC sample. The careful studies on each backgrounds are discussed in the following sections.

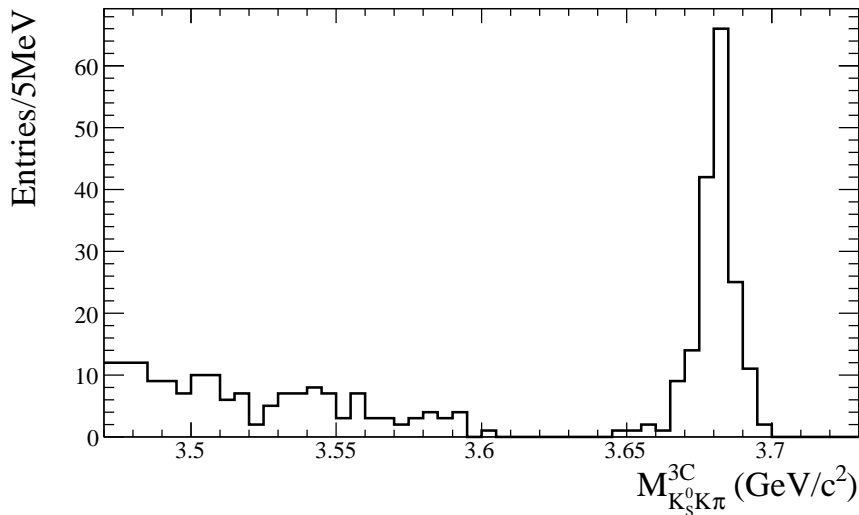


Figure 9: The mass spectrum for the backgrounds predicted by inclusive MC sample.

Table 3: The topology and entries of the backgrounds estimated by the inclusive MC sample in different mass regions.

mass region (GeV/c ²)	3.47 ~ 3.6 (χ_{cJ} mass region)	3.6 ~ 3.66 ($\eta_c(2S)$ mass region)	3.66 ~ 3.7
N($\psi' \rightarrow \pi^0 K_S^0 K^\pm \pi^\mp$)	136	1	0
N($\psi' \rightarrow K_S^0 K^\pm \pi^\mp$)	1	4	167
N($\psi' \rightarrow \gamma 4prong$)	7	0	0
N($\psi' \rightarrow \gamma \chi_{c2} \rightarrow \gamma K_S^0 K_S^0$)	8	0	0
N(others)	10	0	3

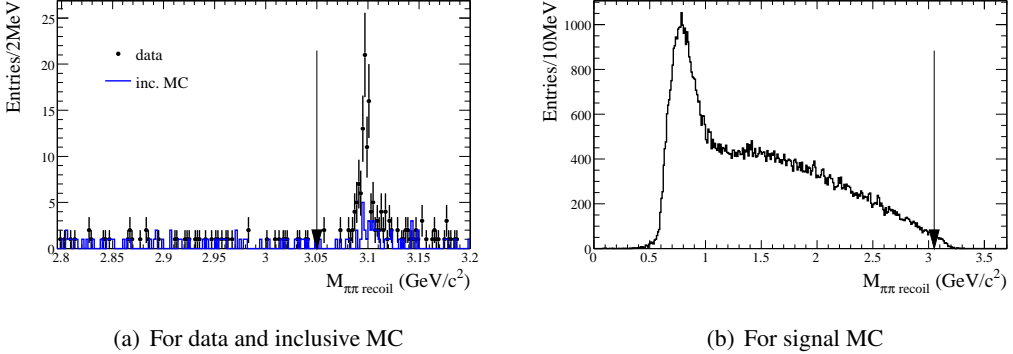


Figure 10: The $\pi^+\pi^-$ recoil mass after the event selection for $\gamma K_S^0 K^\pm \pi^\mp$ described in Section 3.

4.2.1 Background from $\psi' \rightarrow X + J/\psi, J/\psi \rightarrow l^+l^-$

Among ψ' decay modes, the hadronic transition between ψ' and J/ψ has a big fraction that even a very small probability for these events to survive can make a significant contamination. The leading decay modes for this kind of backgrounds are $\psi' \rightarrow \pi^+\pi^-J/\psi$ with $J/\psi \rightarrow l^+l^-$ and $\eta J/\psi$ with $\eta \rightarrow \pi^+\pi^-\pi^0, J/\psi \rightarrow l^+l^-$, because there are 4 charged tracks in the final states. If all the final states are assumed to be pions, there will be a clear J/ψ signal on the recoil mass spectrum of all ' $\pi^+\pi^-$ ' pair (for the events from $\eta J/\psi$ with $\eta \rightarrow \pi^+\pi^-\pi^0, J/\psi \rightarrow l^+l^-$, the J/ψ signal will spread and become larger than J/ψ mass) as shown in Figure 10(a). While there is only a small fraction of events around the J/ψ mass on the recoil mass for the signal $\psi' \rightarrow \gamma\eta_c(2S), \eta_c(2S) \rightarrow K_S^0 K^\pm \pi^\mp$ as shown in Figure 10(b). So the recoil mass of any $\pi^+\pi^-$ pair is required to be less than $3.05\text{GeV}/c^2$ to reject the background from $\psi' \rightarrow X + J/\psi, J/\psi \rightarrow l^+l^-$, and there is only 2.4% relative loss for signal. All the studies described in the following sections will based on the complete event selection including the J/ψ veto condition.

4.2.2 Background from $K_S^0 K^\pm \pi^\mp(\gamma_{FSR})$

As the energy of the transition photon for $\psi' \rightarrow \gamma\eta_c(2S)$ is about 50MeV, which is so soft that the events from $\psi' \rightarrow K_S^0 K^\pm \pi^\mp$ (also $e^+e^- \rightarrow \gamma^* \rightarrow K_S^0 K^\pm \pi^\mp$, but less which will be shown in Section 4.2.4) can contaminate the signal by fake photons or real soft photons from FSR. The final mass spectrum for $\psi' \rightarrow K^*(892)\bar{K} + c.c. \rightarrow K_S^0 K^\pm \pi^\mp(\gamma_{FSR})$ MC is shown in Figure 11, where the photons from FSR are generated by PHOTOS [8], and the number of events is normalized to data according to the previous measurement [9]. According to the plot, there is a big bump around ψ' mass where the events with fake photons dominate, and a smooth tail expanded in the $\eta_c(2S)$ mass region where the FSR events dominate. The estimated number of events in $\eta_c(2S)$ mass region is 6.6 ± 1.4 . But from this spectrum, one can find that the simulation of FSR is quite important in the estimation of this background and need to be checked in data.

The events from $\psi' \rightarrow \gamma\chi_{c1}, \chi_{c1} \rightarrow K_S^0 K^\pm \pi^\mp(\gamma_{FSR})$ are taken as the sample to check FSR in data. This is motivated by two facts, one is this signal not far from $\eta_c(2S)$, the other is the large statistics. Of cause χ_{c2} signal is closer to $\eta_c(2S)$, but it has much less statistics and its FSR "tail" would be affected by χ_{c1} events. To select these FSR events, the corresponding event selection is for $\gamma\gamma K_S^0 K^\pm \pi^\mp$, which is very similar to the one for $\gamma K_S^0 K^\pm \pi^\mp$ except two photons are required in the final states. The two photons will be called the harder photon and the softer photon according to the energy respectively. Similarly the

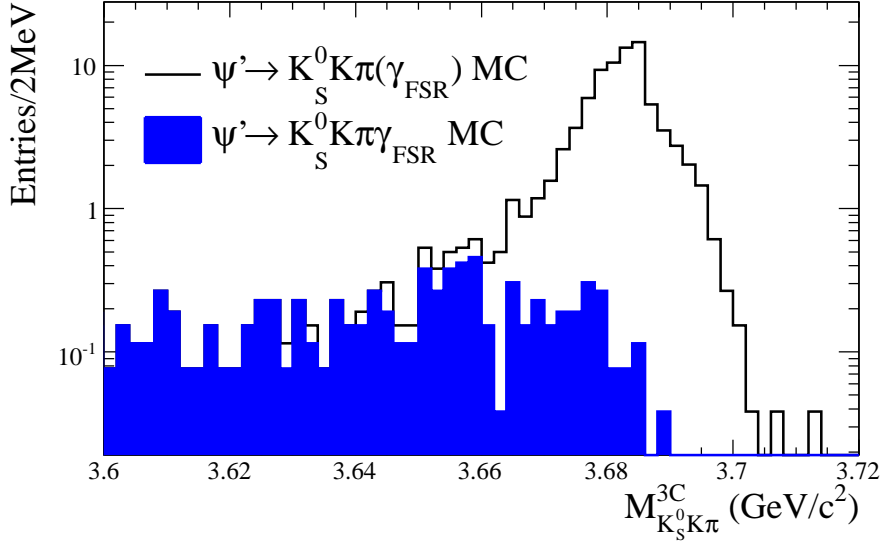


Figure 11: The invariant mass of $K_S^0 K \pi$ for $\psi' \rightarrow K_S^0 K^\pm \pi^\mp (\gamma_{FSR})$, where the empty histogram is for the sum of the $K_S^0 K^\pm \pi^\mp$ events with and without FSR, and the blue histogram is for FSR events only.

4C kinematic fits for $\gamma\gamma K_S^0 K^\pm \pi^\mp$ are used to select events where $\chi^2_{\gamma\gamma K_S^0 K^\pm \pi^\mp 4C} < 50$ is applied, and the 3C kinematic fits are used to calculate the invariant mass of final states (the energy of the softer photon is not used as input in the 3C kinematic fits). As expected, the main background is from $\pi^0 K_S^0 K^\pm \pi^\mp$ with $\pi^0 \rightarrow \gamma\gamma$, and the invariant mass of the two photons after 3C fits are shown in Figure 12 for signal MC , inclusive MC and data. In Figure 12(b) a significant π^0 peak is observed. As a consequence, the events to be used for FSR study are required to have the invariant mass of the two photons $M_{\gamma\gamma}$ outside of the π^0 peak: $M_{\gamma\gamma} < 0.1\text{GeV}/c^2$ or $M_{\gamma\gamma} > 0.155\text{GeV}/c^2$

After the event selection, the backgrounds predicted by inclusive MC are at $(15 \pm 2)\%$ level respect to data around χ_{c1} mass region ($3.35\text{GeV}/c^2 < M_{K_S^0 K^\pm \pi^\mp} < 3.53\text{GeV}/c^2$). The invariant mass of $K_S^0 K^\pm \pi^\mp$ versus the invariant mass of $K_S^0 K^\pm \pi^\mp \gamma_{soft}$ for signal MC, inclusive MC and data are shown in Figure 13. Besides the spot for the events from $\chi_{c1} \rightarrow K_S^0 K^\pm \pi^\mp$ with fake photons shown in Figure 13(a), there is a "tail" from FSR marked by a black box, these FSR events spread in $M_{K_S^0 K \pi}$ but peak in $M_{K_S^0 K \pi \gamma_{soft}}$ at the χ_{c1} mass. The FSR tail is also observed in data (Figure 13(c)). So the FSR rate for data and MC can be compared using the events on the tail.

The projected mass $M_{K_S^0 K \pi}$ for MC, inclusive MC and data are shown on the top row of Figure 14. The energy distributions for the hard photons and soft photons are shown in Figure 15. According to the distribution of the signal MC (Figure 14 top left), the FSR tail is low and smooth. But if the softer photon is added back to the hadronic final states of the events on the FSR tail ($3.35\text{GeV}/c^2 < M_{K_S^0 K \pi} < 3.48\text{GeV}/c^2$) to calculate the invariant mass, a clear peak at χ_{c1} is observed in the mass spectrum of $K_S^0 K \pi \gamma_{soft}$ as shown on the bottom left of Figure 14. And the same mass distribution are also produced for inclusive MC and data, which are illustrated on the bottom middle and bottom right of Figure 14.

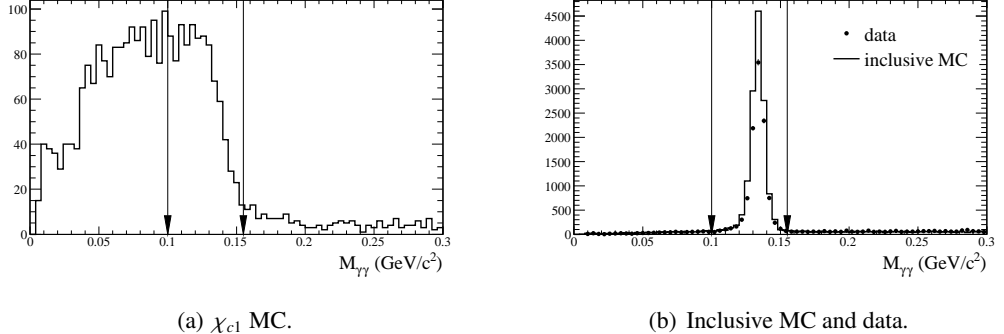


Figure 12: Invariant mass of the two photons for $\gamma\gamma K_S^0 K\pi$ candidates.

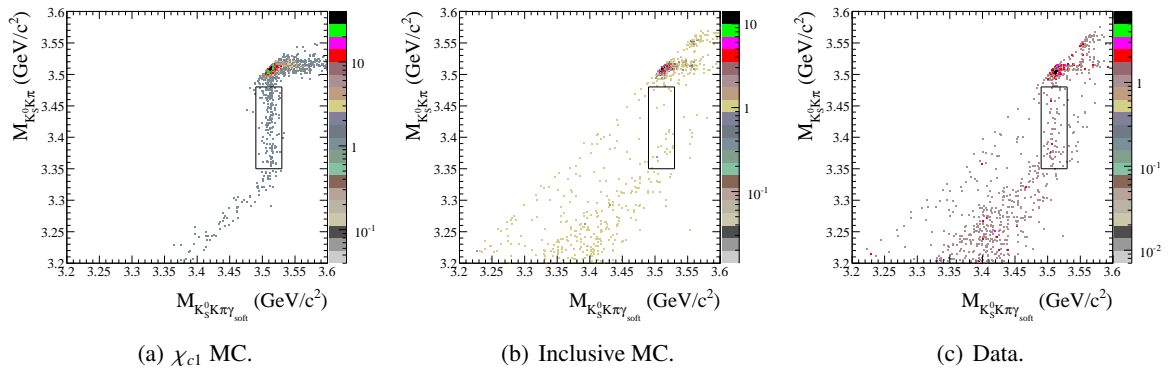


Figure 13: The 2D plots $M_{K_S^0 K\pi}$ versus $M_{K_S^0 K\pi \gamma_{soft}}$ for the events surviving the $\gamma\gamma K_S^0 K\pi$ selection. (*For the inclusive MC sample, the FSR photons are generated, but the interactions between FSR photons and detectors are not simulated.)

Then a ratio R_{FSR} is defined to indicate the FSR rate in MC and data after event selection:

$$R_{FSR} = \frac{N_{FSR}}{N_{noFSR}}, \quad (1)$$

where N_{FSR} is the number of FSR events which are on the FSR tail but with $M_{K_S^0 K\pi\gamma_{soft}}$ under the χ_{c1} peak (i.e. events with $M_{K_S^0 K\pi} \in [3.35, 3.48]\text{GeV}/c^2$, $M_{K_S^0 K\pi\gamma_{soft}} \in [3.49, 3.53]\text{GeV}/c^2$), N_{noFSR} is the number of the events without significant FSR (i.e. events having $M_{K_S^0 K\pi}$ under the χ_{c1} peak $M_{K_S^0 K\pi} \in [3.49, 3.53]\text{GeV}/c^2$). This ratio is an effective quantity reflecting the FSR event rate respect to the events survived by fake photons after the event selection. This quantity for signal MC can be calculated directly: $R_{FSR}^{MC} = 0.103 \pm 0.009$. And the value for data is calculated in this way:

$$R_{FSR}^{data} = \frac{N_{FSR}^{obs} - N_{FSR}^{BG}}{N_{noFSR}^{obs} - N_{noFSR}^{BG}} = 0.136 \pm 0.033, \quad (2)$$

where N_{FSR}^{obs} is the observed number of FSR events in data, N_{noFSR}^{obs} is the observed number of non-FSR events in data, N_{FSR}^{BG} and N_{noFSR}^{BG} are the number of background events estimated by the inclusive MC sample for 'FSR' events and 'non-FSR' events respectively. The systematic bias of this method could come from the resolution difference between data and MC, the uncertainty of background estimation. The ratio about FSR of data to MC $\frac{R_{FSR}^{data}}{R_{FSR}^{MC}} = 1.33 \pm 0.34$ is obtained from this study, which means that effective FSR rates for data is about 30% larger than MC, but the error is also large, so the difference is not significant which is only 1 standard deviation. With the same method, the ratio of effective FSR ratio for data and MC can also be studied in other decay modes, like $\psi' \rightarrow \gamma\pi^+\pi^-K^+K^-$ and $\psi' \rightarrow \gamma 2(\pi^+\pi^-)$ [14], which are $1.37 \pm 0.08 \pm 0.02$ and $1.63 \pm 0.07 \pm 0.03$ respectively. Because the radiation from pions dominate the contribution of FSR, one can get the approximate relationship $r^2 = 1.37$ and $r^4 = 1.63$, where $r = \frac{R_{FSR}^{data}}{R_{FSR}^{MC}}$ is the ratio for single charged pion. The results from different decay modes are summarized as the following: $r_{\gamma K_S^0 K\pi} = 1.33 \pm 0.34$, $r_{\gamma\pi^+\pi^-K^+K^-} = 1.170 \pm 0.035$ and $r_{\gamma 2(\pi^+\pi^-)} = 1.130 \pm 0.013$. The combined result is $r = 1.135 \pm 0.012$. So the background from $K_S^0 K^\pm\pi^\mp(\gamma_{FSR})$ contribute $6.6 \times 1.135 = 7.5 \pm 1.6$ events in $\eta_c(2S)$ mass region.

4.2.3 Background from $\pi^0 K_S^0 K^\pm\pi^\mp$

With all these event selection criteria, the events from $\pi^0 K_S^0 K^\pm\pi^\mp$ can still contaminate the $\gamma K_S^0 K^\pm\pi^\mp$ candidates if one of the two photons from π^0 decay is soft. This means that π^0 veto can not be an efficient way to suppress the remained $\pi^0 K_S^0 K^\pm\pi^\mp$ background, because only a small fraction of these soft photons can be reconstructed.

But the mass spectrum for $\pi^0 K_S^0 K^\pm\pi^\mp$ background can be estimated by measuring $\pi^0 K_S^0 K^\pm\pi^\mp$ in data and scaling the measured mass spectrum to the ' $\gamma K_S^0 K^\pm\pi^\mp$ ' case according to the simulation. With a similar event selection procedure:

- 4 charged tracks with total charge zero, and at least 2 photons
- one and only one good K_S^0 candidate
- a list for the photon pair from π^0 is made by performing the 1C fit on any photon pair to the π^0 mass, where $\chi^2_{(\pi^0 \rightarrow \gamma\gamma)1C} < 10$ is required

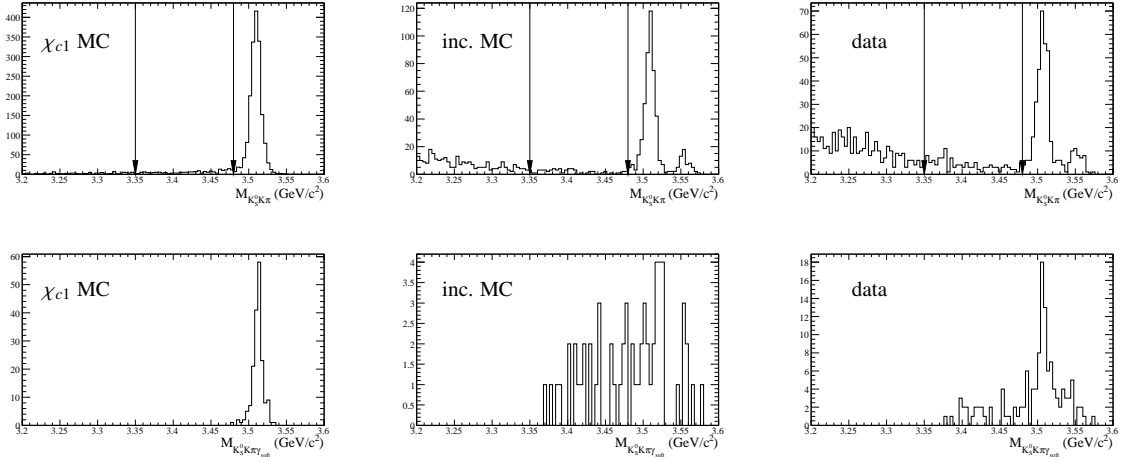


Figure 14: Top: the $M_{K_S^0 K\pi}$ distribution for the events surviving the $\gamma\gamma K_S^0 K\pi$ selection. Bottom: the $M_{K_S^0 K\pi \gamma_{soft}}$ distribution for the events with $M_{K_S^0 K\pi}$ between 3.35GeV and 3.48GeV. (* For the inclusive MC sample, FSR photons are generated, but the interactions between FSR photons and detectors are not simulated.)

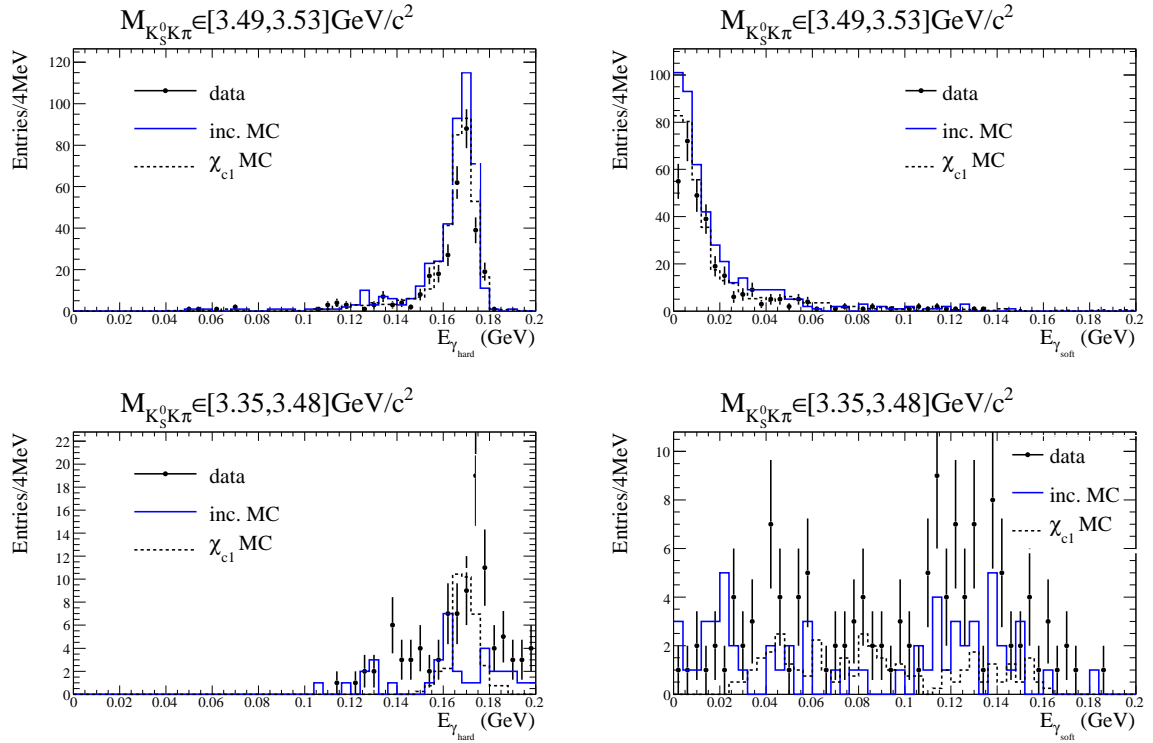


Figure 15: The energy distribution for the hard photons (left) and the soft photons (right). Top: the events under the χ_{c1} peak ($M_{K_S^0 K\pi} \in [3.49, 3.53] \text{ GeV}/c^2$), bottom: the events on the FSR tail ($M_{K_S^0 K\pi} \in [3.35, 3.48] \text{ GeV}/c^2$).

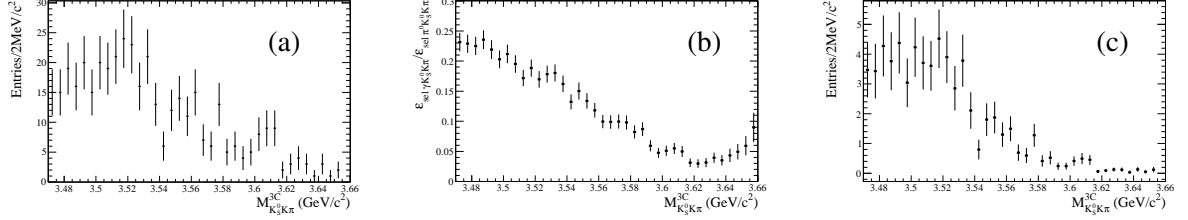


Figure 16: The estimation of the background from $\pi^0 K_S^0 K^\pm \pi^\mp$. (a) The mass spectrum for $\pi^0 K_S^0 K^\pm \pi^\mp$ selected in data, (b) The ratio of the efficiencies of $\gamma K_S^0 K^\pm \pi^\mp$ selection and $\pi^0 K_S^0 K^\pm \pi^\mp$ selection, (c) The estimated mass spectrum for $\pi^0 K_S^0 K^\pm \pi^\mp$.

- the 5C kinematic fits are performed on the final states to $\pi^0 K_S^0 K^\pm \pi^\mp, \pi^0 \rightarrow \gamma\gamma$ by looping all the photon pair in the list, the best photon pairs from π^0 are kept respectively for the two cases $\pi^0 K_S^0 K^+ \pi^-$ and $\pi^0 K_S^0 K^- \pi^+$
- the final state $\pi^0 K_S^0 K^+ \pi^-$ or $\pi^0 K_S^0 K^- \pi^+$ is determined by the smaller $\chi^2_{\pi^0 K_S^0 K\pi} = \chi^2_{(\pi^0 K_S^0 K\pi)5C} + \chi^2_{K\text{-ID}} + \chi^2_{\pi\text{-ID}}$
- $\chi^2_{(\pi^0 K_S^0 K\pi)5C} < 15$

$\pi^0 K_S^0 K^\pm \pi^\mp$ events are obtained, and the background level is about 2% that is estimated by the inclusive MC. But the mass of $K_S^0 K^\pm \pi^\mp$ for selected $\pi^0 K_S^0 K^\pm \pi^\mp$ events is still calculated in the same way as signal, which is shown in Figure 16(a). According to the simulation with large statistics for $\pi^0 K_S^0 K^\pm \pi^\mp$, the efficiency ratio of the two event selections (the selections for $\gamma K_S^0 K^\pm \pi^\mp$ and $\pi^0 K_S^0 K^\pm \pi^\mp$) as a function of $M_{K_S^0 K\pi}^3C$ is obtained in Figure 16(b). Finally, the mass spectrum for the background in selected " $\gamma K_S^0 K^\pm \pi^\mp$ " data sample is estimated by scaling the measured mass spectrum with the efficiency ratio spectrum. As shown in Figure 16(c), the mass spectrum for the background from $\pi^0 K_S^0 K^\pm \pi^\mp$ decreases smoothly without special structure, and only contribute 2.2 events in $\eta_c(2S)$ mass region.

4.2.4 Background from continuum

The background from continuum can be estimated by the data sample taken at $3.65\text{GeV}/c^2$. After the same selection, the mass spectrum for the continuum data is shown in Figure 17(a). The scale factor for the whole mass spectrum is

$$f_{continuum} = \frac{156.4 \text{ pb}^{-1}}{42.6 \text{ pb}^{-1}} \cdot \left(\frac{3.65 \text{ GeV}}{3.686 \text{ GeV}} \right)^2 = 3.6, \quad (3)$$

where 156.4pb^{-1} and 42.6pb^{-1} are the integrated luminosity at 3.686GeV and 3.65GeV respectively, $(\frac{3.65}{3.686}\text{GeV})^2$ is for the cross section difference between the two energy points. Considering the energy difference, the mass is shifted according to the following operation:

$$m \rightarrow a(m - m_0) + m_0, \quad (4)$$

where $m_0 = 1.13086 \text{ GeV}/c^2$ is the mass threshold for $K_S^0 K\pi$ which should not be shifted, the coefficient $a = (3.686 - m_0)/(3.65 - m_0) = 1.0143$ makes sure the events at $3.65 \text{ GeV}/c^2$ are shifted to $3.686 \text{ GeV}/c^2$. The shifted and scaled mass spectrum for the continuum contribution is shown in Figure 17(b). The estimated number of backgrounds from continuum contribution is 7.2 ± 5.1 in $\eta_c(2S)$ mass region.

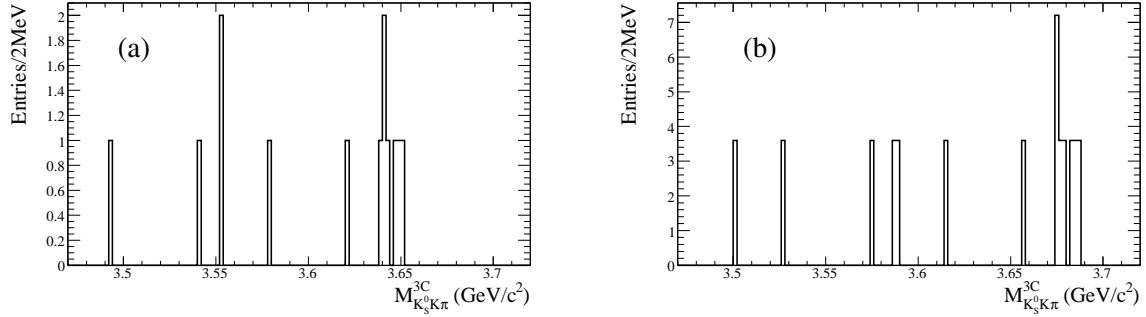


Figure 17: (a) The measured mass spectrum for the continuum data collected at 3.65 GeV; (b) the shifted and scaled mass spectrum for the estimation of the continuum contribution.

4.2.5 Summary of the backgrounds for $\gamma K_S^0 K^\pm \pi^\mp$

The mass spectrum outside of the $\eta_c(2S)$ box and the sum mass spectrum of all the estimated backgrounds and χ_{cJ} contributions are shown in Figure 18, which shows that the estimated backgrounds can describe data well in the vicinity of the $\eta_c(2S)$ mass region which convince us to open the mass box. The same estimate of backgrounds predicts $(7.5 + 2.2 + 7.2) = 17 \pm 6$ events inside the mass box, while about 80 events are observed inside of the mass box, so there must be something new in data!

5 Efficiency of the event selection and systematic uncertainties

5.1 Over all efficiency

A MC sample with 100000 statistics for $\psi' \rightarrow \gamma \eta_c(2S)$, $\eta_c(2S) \rightarrow K_S^0 K^\pm \pi^\mp$ is generated to study the efficiency of the event selection, where the polar angle of the transition photon follows $P(\cos \theta) = 1 + \cos^2 \theta$ distribution, and $\eta_c(2S) \rightarrow K_S^0 K^\pm \pi^\mp$ is generated according to phase space model. After the complete event selection, the mass spectrum for this signal MC sample is shown in Figure 23. The efficiency of the event selection for signal events is $(23.16 \pm 0.13)\%$ which is estimated by the full simulation.

The possible systematic bias from the generation of the signal MC sample is that the intermediate states in the $\eta_c(2S) \rightarrow K_S^0 K^\pm \pi^\mp$ decay are not considered. But this can be estimated from the $\eta_c \rightarrow K_S^0 K^\pm \pi^\mp$ decay. The mass spectrum of $K_S^0 K^\pm \pi^\mp$ around η_c and the dalitz plot for the events under the η_c mass peak are shown in Figure 19 and Figure 20 respectively. The components of the intermediate states are likely $K_0^*(1430)\bar{K}$, $K_2^*(1430)\bar{K}$, $a_0(980)^\pm \pi^\mp$, $a_2(1320)^\pm \pi^\mp$ and $K^*(892)\bar{K}$. By fitting the dalitz plots with all the possible components from MC (Figure 21), one can get the relative fractions and accordingly regenerate $\eta_c(2S) \rightarrow K_S^0 K^\pm \pi^\mp$ MC samples. The efficiency as a function of $M_{K_S^0 K^\pm \pi^\mp}^{3C}$ using the regenerated MC sample is shown in Figure 22.

And the systematic uncertainties on the efficiency are studied in the following sections.

5.2 Photon efficiency

The uncertainty due to photon detection and photon conversion is 1% per photon [13]. This is determined from studies of photon detection efficiencies in well understood decays such as $J/\psi \rightarrow \rho^0 \pi^0$, $\rho^0 \rightarrow \pi^+ \pi^-$,

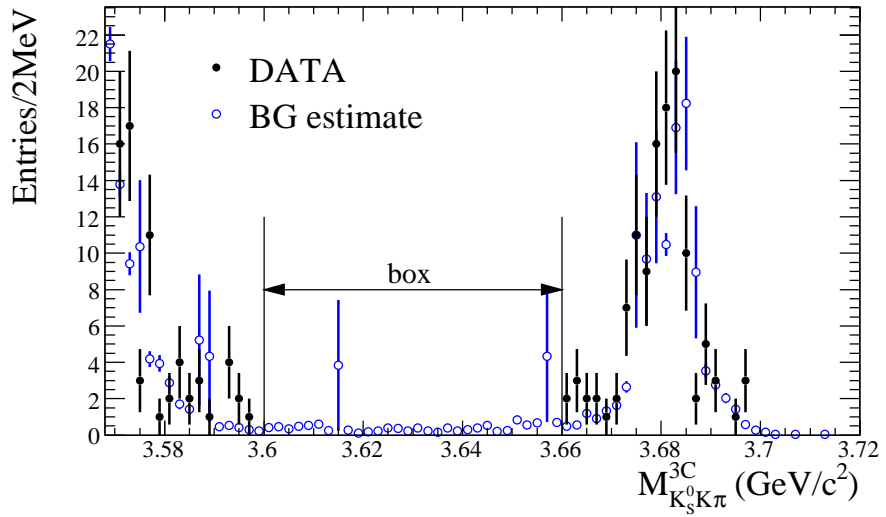


Figure 18: The mass spectra for data outside of the $\eta_c(2S)$ box and the estimated backgrounds.

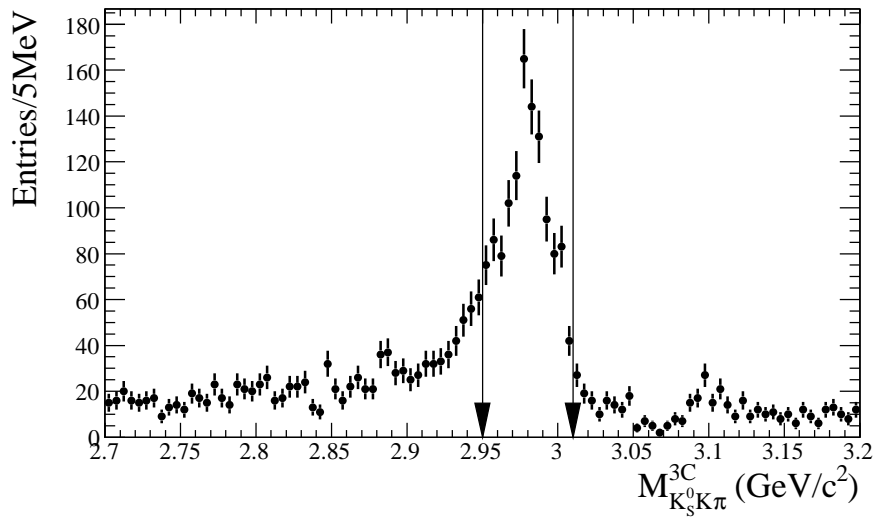


Figure 19: The invariant mass of $K_s^0 K^\pm \pi^\mp$ around η_c .

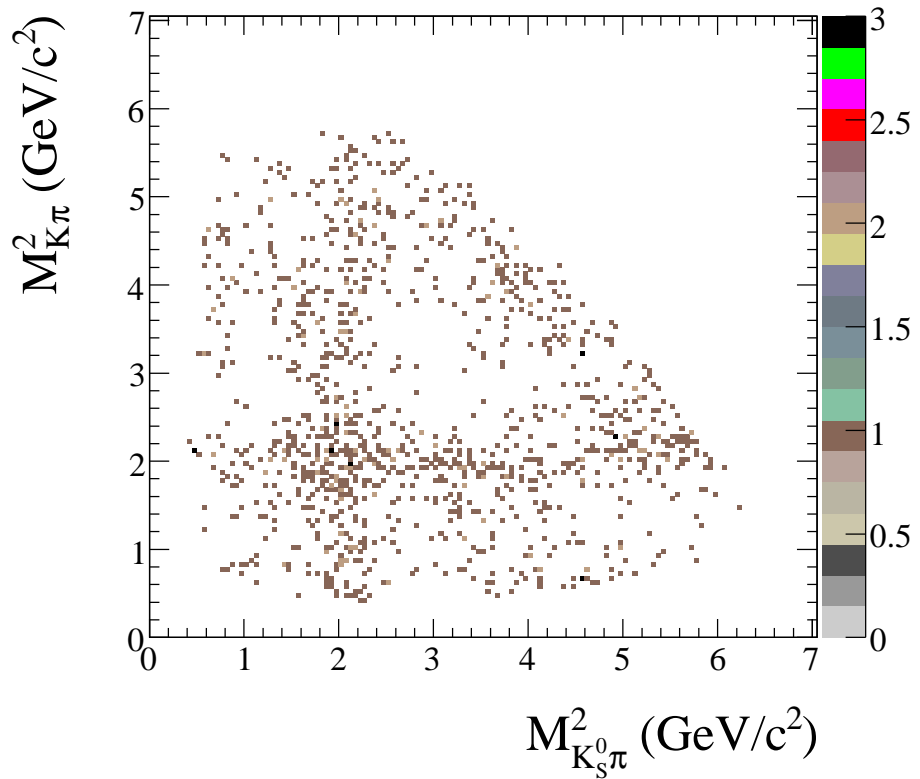


Figure 20: The dalitz plot for the events under the η_c mass peak by requiring $M_{K_s^0 K^\pm \pi^\mp}^{3C} \in [2.95, 3.01]\text{GeV}/c^2$.

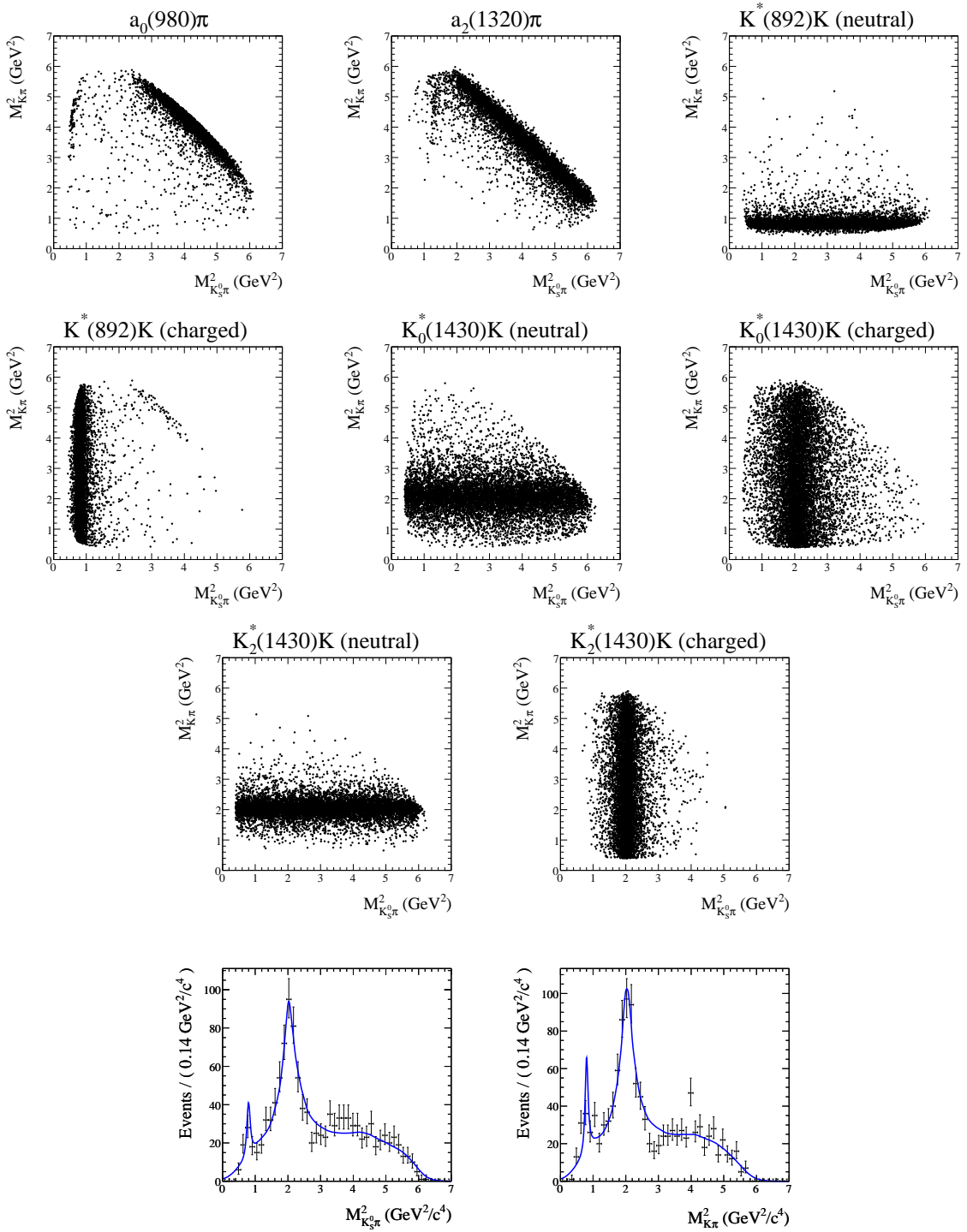


Figure 21: Fitting of the dalitz plot for $\eta_c \rightarrow K_S^0 K^\pm \pi^\mp$ data. The first 8 plots show the dalitz plots ($M_{K^\pm \pi^\mp}^2$ vs. $M_{K_S^0 \pi^\pm}^2$) for different components and the last two are the projections of the fitting results.

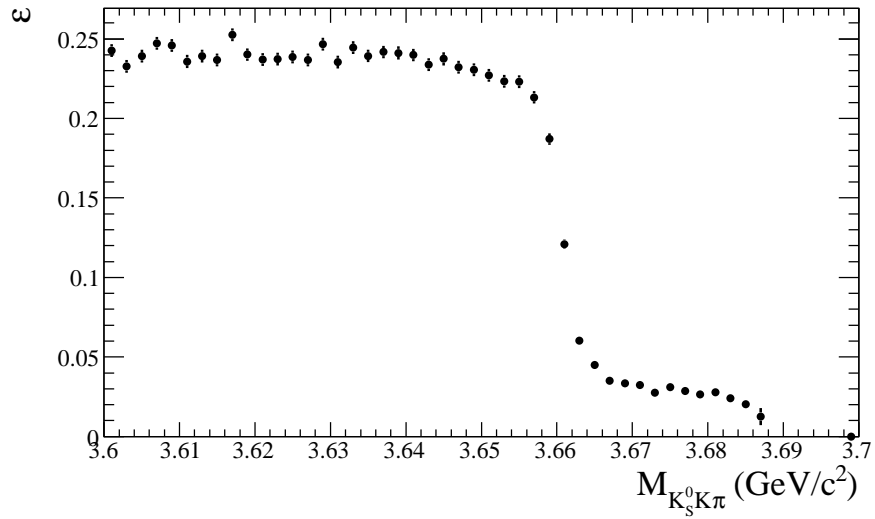


Figure 22: The efficiency as a function of $K_s^0 K^\pm \pi^\mp$ mass for the $\eta_c(2S)$ signal MC with possible intermediate states determined from $\eta_c \rightarrow K_s^0 K^\pm \pi^\mp$ decay in data.

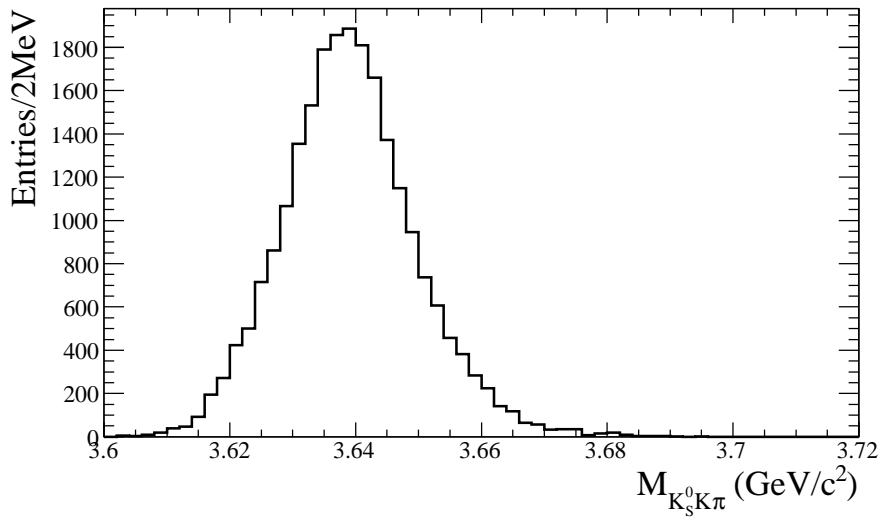


Figure 23: The invariant mass of $K_s^0 K^\pm \pi^\mp$ from 3C kinematic fits for $\psi' \rightarrow \gamma \eta_c(2S)$, $\eta_c(2S) \rightarrow K_s^0 K^\pm \pi^\mp$ MC.

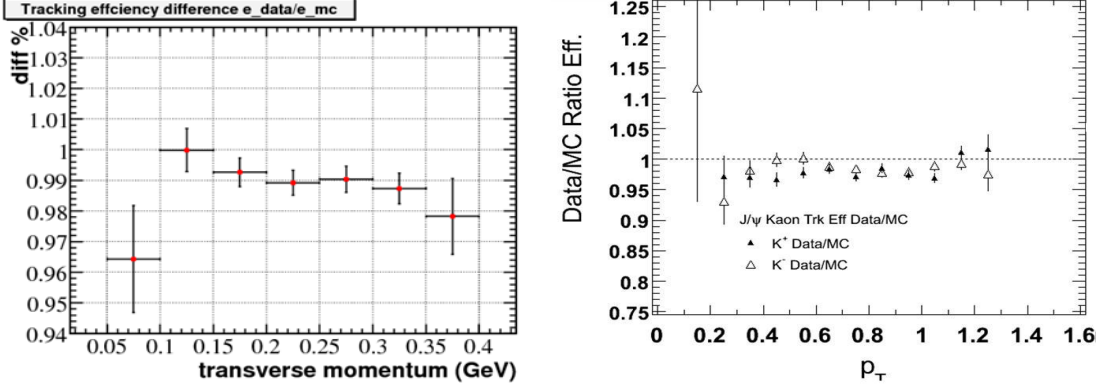


Figure 24: The difference in the tracking efficiency between data and MC as a function of transverse momentum for pions (left) and kaons (right).

$\pi^0 \rightarrow \gamma\gamma$ and study of photon conversion via $e^+e^- \rightarrow \gamma\gamma$.

5.3 Efficiency for K_S^0 reconstruction

The complete efficiency for K_S^0 reconstruction consists of three parts: the geometric acceptance, tracking efficiency and the efficiency for the decay length request $L_{decay} > 0.5\text{cm}$. The first part geometric acceptance can be estimated using MC sample. The other two were studied in the process $J/\psi \rightarrow K^* \bar{K}^0 + c.c.$ [10], where K^* is reconstructed through the process $K^* \rightarrow K^\pm \pi^\mp$, then the amount of K^* (i.e. the number of K^0) can be obtained by fitting the momentum spectrum of K^* and subsequently the expected number of $K_S^0 \rightarrow \pi^+\pi^-$ (half of N_{K^0}) is determined. With this sample, one can check the possibility to reconstruct the K_S^0 from a pair of pions. The difference between data and MC is found to be 3.5%.

5.4 Tracking efficiency for K, π from IP

The tracking efficiency for π as a function of transverse momentum (the difference between data and MC is shown on the left plot in Figure 24, the difference for the pion tracks with higher momenta is assumed conservatively to be 1.5%) has been studied in the processes $\psi' \rightarrow \pi^+\pi^- J/\psi$ [11]. Similarly, the tracking efficiency for K as a function of transverse momentum (the right plot in Figure 24 shows the ratio of data over MC) has been studied with the process $J/\psi \rightarrow K_S^0 K^\pm \pi^\mp$ [12]. After sampling the difference in tracking efficiency using the $\eta_c(2S)$ MC sample (the transverse momentum distributions are shown in Figure 25), one can get the difference in tracking efficiency at event level between data and MC less than 2.5%.

5.5 Efficiency for χ^2 cut of kinematic fitting

As already shown in Figure 7(a), there is some difference in the χ^2 distributions of kinematic fitting between data and simulation. And the efficiency for the χ^2 cut of kinematic fitting is estimated by the $\psi' \rightarrow \gamma\chi_{cJ}, \chi_{cJ} \rightarrow K_S^0 K^\pm \pi^\mp$ events which are selected without kinematic fitting as the following:

- at least one good photon, four charged tracks with total charge equals zero

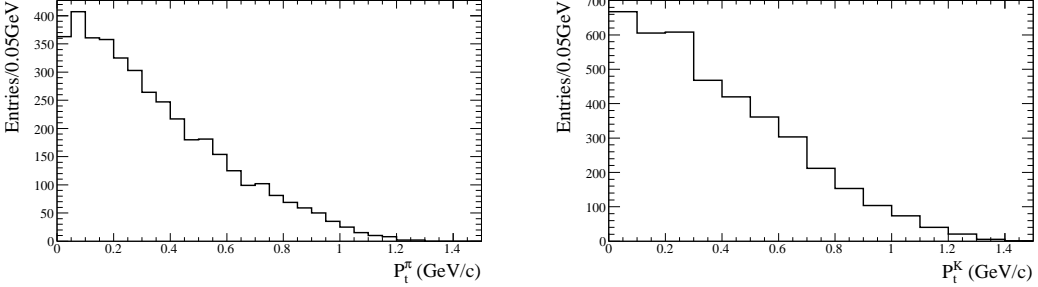


Figure 25: The transverse momentum distributions for π (left) and K (right) in the $\psi' \rightarrow \gamma\eta_c(2S) \rightarrow \gamma K_S^0 K^\pm \pi^\mp$ MC sample.

- one and only one good $K_S^0 \rightarrow \pi^+ \pi^-$ candidate
- the other two charged tracks are identified as kaon and pion respectively
- J/ψ veto $|M_{\pi\pi\text{recoil}} - 3.097| > 5\text{MeV}$
- if the number of photons is larger than one, π^0 veto $M_{\gamma\gamma} \notin [M_{\pi^0} - 15\text{MeV}, M_{\pi^0} + 10\text{MeV}]$ is applied, where $M_{\gamma\gamma}$ is the invariant mass of two photons closest to π^0
- the reconstructed mass of $K_S^0 K\pi$ is required under χ_{cJ} mass peaks: $M_{K_S^0 K\pi} \in [3.5, 3.525]\text{GeV}/c^2$ for χ_{c1} , $M_{K_S^0 K\pi} \in [3.54, 3.58]\text{GeV}/c^2$ for χ_{c2} to reduce the background level

The inclusive MC sample predicts 2% backgrounds for χ_{c1} events ($M_{K_S^0 K\pi} \in [3.5, 3.525]\text{GeV}/c^2$), 5% for χ_{c2} events ($M_{K_S^0 K\pi} \in [3.54, 3.58]\text{GeV}/c^2$). The contribution from backgrounds is subtracted from the χ^2 distribution for data using MC samples. The efficiencies for χ_{c1}, χ_{c2} as a function of χ^2 cut are shown in Figure 26.

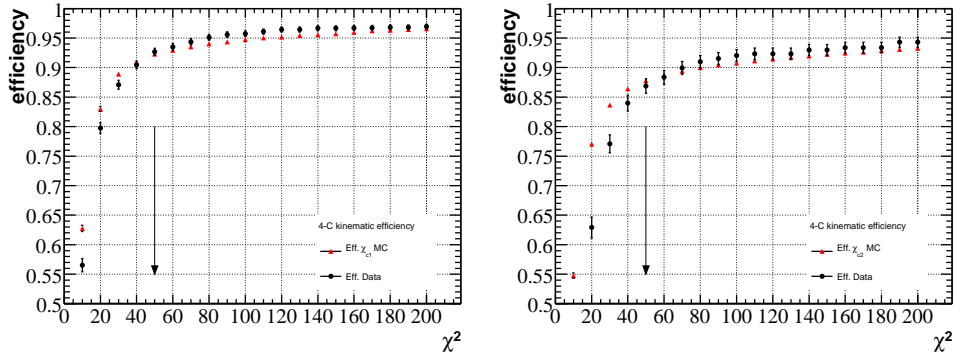


Figure 26: The efficiencies as a function of χ^2 cut for χ_{c1} (left) and χ_{c2} (right) events.

For the used χ^2 cut $\chi_{4C}^2 < 50$, the ratios of efficiencies for data and MC $\epsilon_{data}/\epsilon_{MC}$ are 1.004 ± 0.007 for χ_{c1} and 0.990 ± 0.014 for χ_{c2} . Both of the two ratios are consistent with one. If the ratio is assumed to have a linear dependence of mass, the central value of the ratio is expected to be 0.965 (i.e. 3.5% in

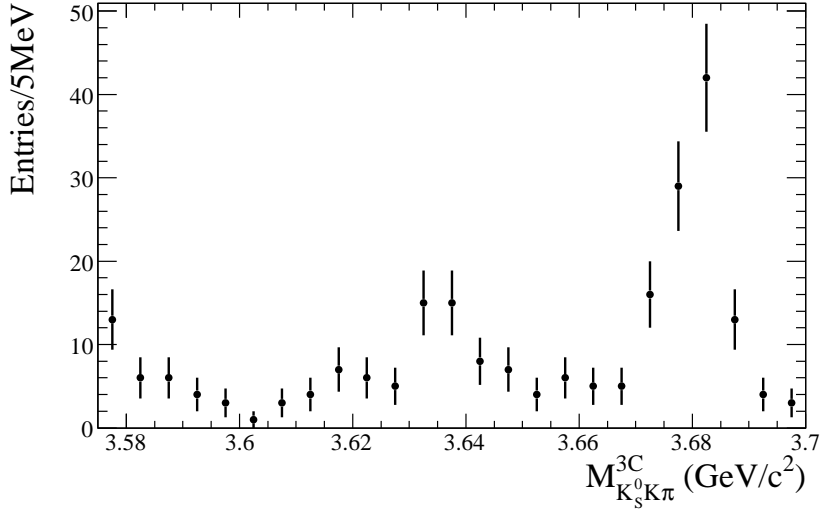


Figure 27: The spectrum of the invariant mass of $K_S^0 K \pm \pi^\mp$ for data in the $\eta_c(2S)$ mass region.

difference) at $3.637\text{GeV}/c^2$. To be conservative, 3.5% is taken as the systematic error for the efficiency of χ^2 cut around $\eta_c(2S)$.

6 Opening the mass box and the fitting of signal

The expected contributions and data are consistent outside the $\eta_c(2S)$ mass region, while there is significant difference between expectation and observation in the $\eta_c(2S)$ mass region. This fact make it interesting that what's the new thing in data? After opening the mass box, a bump is observed around 3635 MeV on the mass spectrum as shown in Figure 27.

A mass spectrum fitting needs to be performed to extract the mass, width and number of events of the observed signal. In order to determine better the background and mass resolution using data, the mass spectrum range is enlarged ($3.47 \sim 3.72\text{GeV}/c^2$) to include χ_{c1} and χ_{c2} events. The resonances χ_{c1} and χ_{c2} will be described simply by a Breit-Wigner convolved with a gaussian in the fitting. The widths for χ_{c1}, χ_{c2} are fixed to the PDG values. The mass resolutions for χ_{c1}, χ_{c2} and $\eta_c(2S)$ are studied with the mass difference between the 3C kinematic fitted mass and the true mass using MC samples, which are shown in Figure 28(a,b,c), and have linear mass dependence with a very small slope (Figure 28(d)). So the mass resolution is required to follow the first order polynomial in the final mass fitting.

The line shape for $\eta_c(2S)$ should be described carefully as its width is not small (about 12 MeV) and the relative variation of E_γ is also large ($\sim 12\text{MeV}/50\text{MeV} > 20\%$). A natural line shape for $\eta_c(2S)$ produced by such a M1 transition is given by

$$(E_\gamma^3 \times BW(m) \times damping(E_\gamma)) \otimes Gauss(0, \sigma), \quad (5)$$

where m is the invariant mass of $K_S^0 K \pi$, $E_\gamma = \frac{m_{\psi'}^2 - m^2}{2m_{\psi'}}$ is the energy of the transition photon in the rest frame of ψ' , $damping(E_\gamma)$ is the function to damp the diverging tail raised by E_γ^3 and $Gauss(0, \sigma)$ is

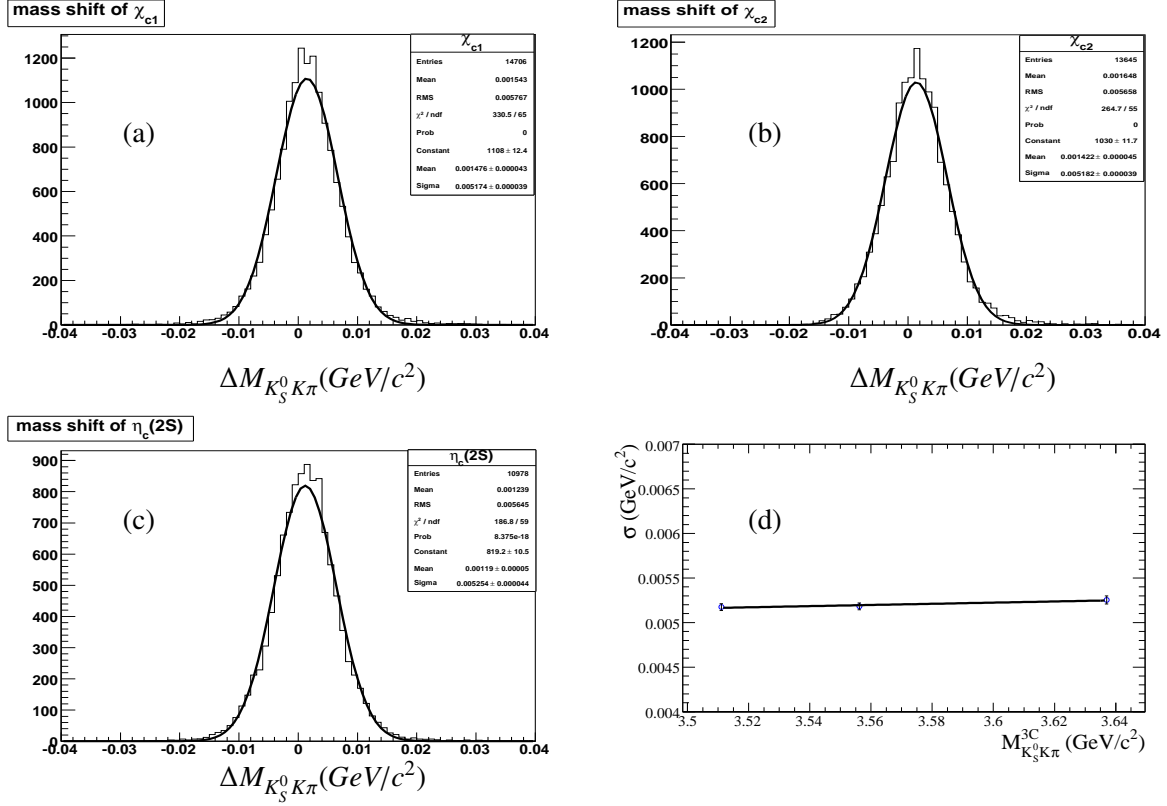


Figure 28: The mass differences between the 3C kinematic fitted mass and the true mass for χ_{c1} MC (a), χ_{c2} MC (b) and $\eta_c(2S)$ MC (c), where the curves show the results of the gaussian fitting. And the mass resolution as a function of mass (d), where the curve is the fitting result using the first order polynomial function.

the gaussian function describing the detector resolution. The possible form of the damping function is somewhat arbitrary, and one suitable function used by KEDR for a similar process is [15]

$$\frac{E_0^2}{E_\gamma E_0 + (E_\gamma - E_0)^2}, \quad (6)$$

where $E_0 = \frac{m_{\psi'}^2 - m_{\eta_c(2S)}^2}{2m_{\psi'}}$ is the peaking energy of the transition photon. Another damping function used by CLEO [16] is inspired by the overlap of wave functions

$$\exp(-E_\gamma^2/\beta^2), \quad (7)$$

with $\beta = (65.0 \pm 2.5)\text{MeV}$ from CLEO's fit. This function (7) is criticized that it has no theoretical justification, which can also be signalled by the unnatural scale of β [17]. So in our analysis, the damping function (6) will be used in the fit to give the final results, and the not-so-justified form (7) will be used to estimate the possible uncertainty caused by the form of damping functions.

The background from the lower mass side is dominated by $\pi^0 K_S^0 K^\pm \pi^\mp$, which is studied in data (see Section 4.2.3). The line shape of this background can be described by Novosibirsk function. The fitting

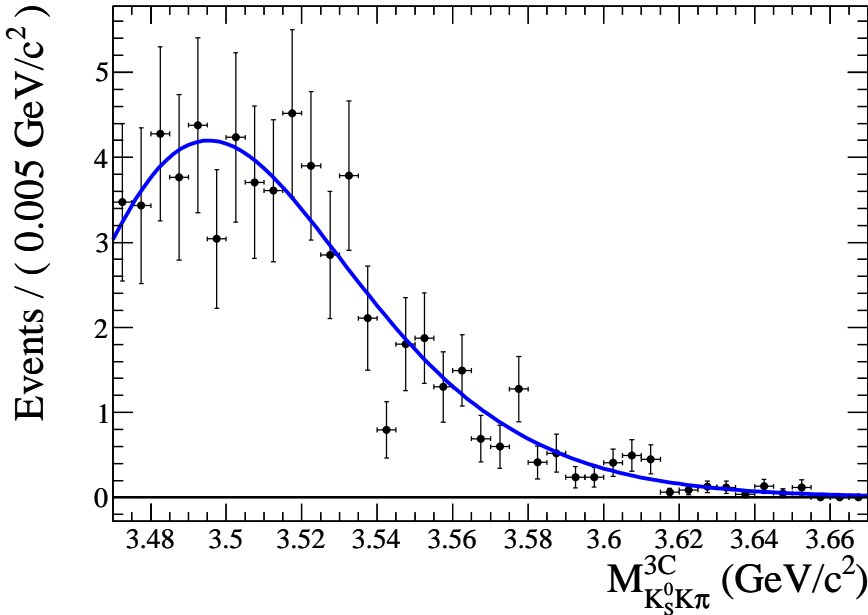


Figure 29: The fitting of the mass spectrum of $\pi^0 K_S^0 K^\pm \pi^\mp$ to Novosibirsk function.

of the corresponding mass spectrum using this function is shown in Figure 29 and the determined shape is fixed in the final mass fitting.

The backgrounds on the higher mass side are $\psi' \rightarrow K_S^0 K^\pm \pi^\mp (\gamma_{FSR})$ and the continuum process actually $e^+ e^- \rightarrow \gamma^*(\gamma_{ISR}) \rightarrow K_S^0 K^\pm \pi^\mp (\gamma_{FSR})$. The events with radiations from either initial states (ISR) or final states (FSR) have similar mass spectrum shape (Figure 30). The $K_S^0 K^\pm \pi^\mp$ events without any radiation but contaminating the signal with fake photons can be produced through ψ' or γ^* , and should have the same line shape of mass spectrum. So the line shape of the mass spectrum for the higher side backgrounds has two basic components: one with radiation and the other without radiation, and both of them are extracted from MC samples (Figure 31). The amounts of the two components in continuum can be obtained by fitting continuum data directly (Figure 32). And the total contribution from $\psi' \rightarrow K_S^0 K^\pm \pi^\mp (\gamma_{FSR})$ is estimated by the MC sample with a proper normalization, where the FSR part is scaled additionally by the data/MC factor for FSR (see Section 4.2.2). All the contributions are summarized in Table 4. The relative ratio of the number of events with radiation over the one without radiation can be determined as 0.43 ± 0.15 , where the correlation between different components is considered in the error calculation. And this ratio will be fixed in the final mass fitting. In order to describe the difference (mass shift and resolution) between data and MC, in the final fitting the component for the events without radiation is represented by the line shape from MC convolved with a gaussian.

So the final function used to fit the data mass spectrum is the sum of the following components:

- $\eta_c(2S)$: a modified theoretical form (5) convolved with a mass dependent gaussian resolution function
- χ_{c1}, χ_{c2} : two Breit-Wigners convolved with the mass dependent gaussian resolution function

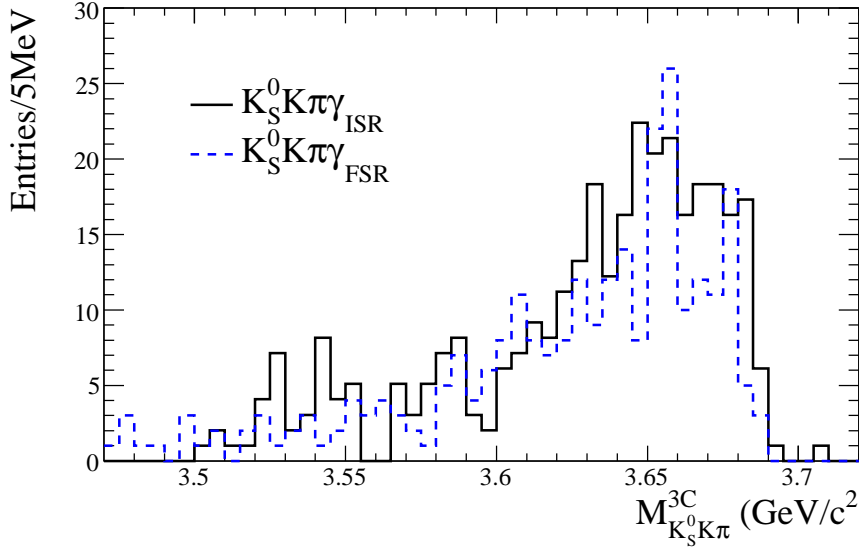


Figure 30: The comparison of the mass spectrum for $K_S^0 K^\pm \pi^\mp \gamma_{ISR}$ and $K_S^0 K^\pm \pi^\mp \gamma_{FSR}$ MC events.

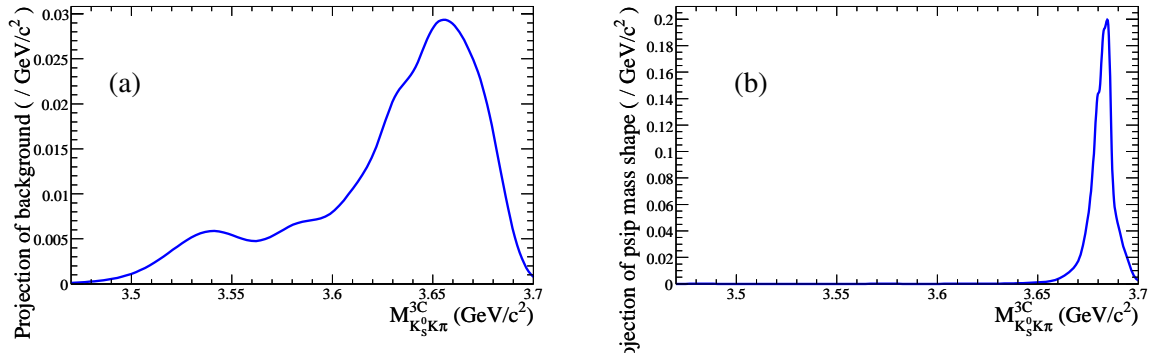


Figure 31: The line shape of the mass spectrum for the events with (a) and without (b) radiation, which are extracted from MC samples.

Table 4: The amounts of $K_S^0 K\pi$ events with and without radiation.

processes	$K_S^0 K\pi$	$K_S^0 K\pi + \gamma_{FSR} \text{ or } ISR$
$\psi' \rightarrow K_S^0 K^\pm \pi^\mp (\gamma_{FSR})$	81 ± 16	12.4 ± 2.4
$e^+ e^- \rightarrow \gamma^*(\gamma_{ISR}) \rightarrow K_S^0 K^\pm \pi^\mp (\gamma_{ISR})$	19.4 ± 9.7	31 ± 12

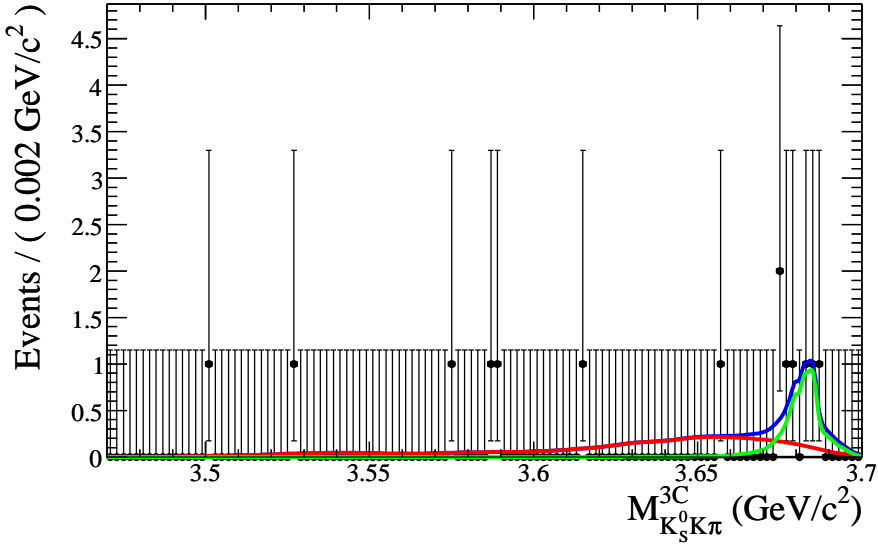


Figure 32: The fitting of the continuum mass spectrum to the two basic components described in the text.

- background from $\pi^0 K_s^0 K^\pm \pi^\mp$: a Novosibirsk function, the parameters of which is fixed to the fitting result shown in Figure 29
- background from $K_s^0 K^\pm \pi^\mp$ with and without radiation, where the ratio of two parts is fixed as already described

Likelihood method is used in the fitting. With the statistics we have, the width of $\eta_c(2S)$ can not be well determined (see Fit 1 in Table 5 and the top plot in Figure 33). With the recent measurements using two-photon processes from Babar [18], Belle [19] and the average from precious experiments [5], one can get the best average value for the width of $\eta_c(2S)$ to be 12 ± 3 MeV. So finally, the width of $\eta_c(2S)$ is decided to be fixed to this best world average value. Fitting of the mass spectrum with the fixed width of $\eta_c(2S)$ is shown in Figure 33 (bottom). The fitting results are summarized in Table 5, where the Fit 2 gives the final result. The statistical significance of the $\eta_c(2S)$ signal is calculated from the difference between the likelihood values of the fitting with and without the signal, which is 6.2σ . The dominant systematic uncertainty which can change the significance comes from the background shape, precisely the relative ratio of the number of $K_s^0 K^\pm \pi^\mp$ events with and without radiation. Even for the worst case (the ratio $(0.43+0.15=0.58)$), the significance is about 5.23σ . So with systematic error considered, the statistical significance can not be less than 5.2σ .

7 Consistency checks

- **Consistency of N_{signal} between the results from estimation and fitting**

The estimated number of signal events is $N_{signal}^{estimate} = 80 - 17 = 63 \pm 9 \pm 6$ in the mass range $3.6 \sim 3.66 \text{ GeV}/c^2$ (80 is the observed number of events, 17 is the estimated number of background events), and the fitted number of signal events including systematics is $N_{signal}^{fitting} = 47.5 \pm 9.4 \pm 8.6 =$

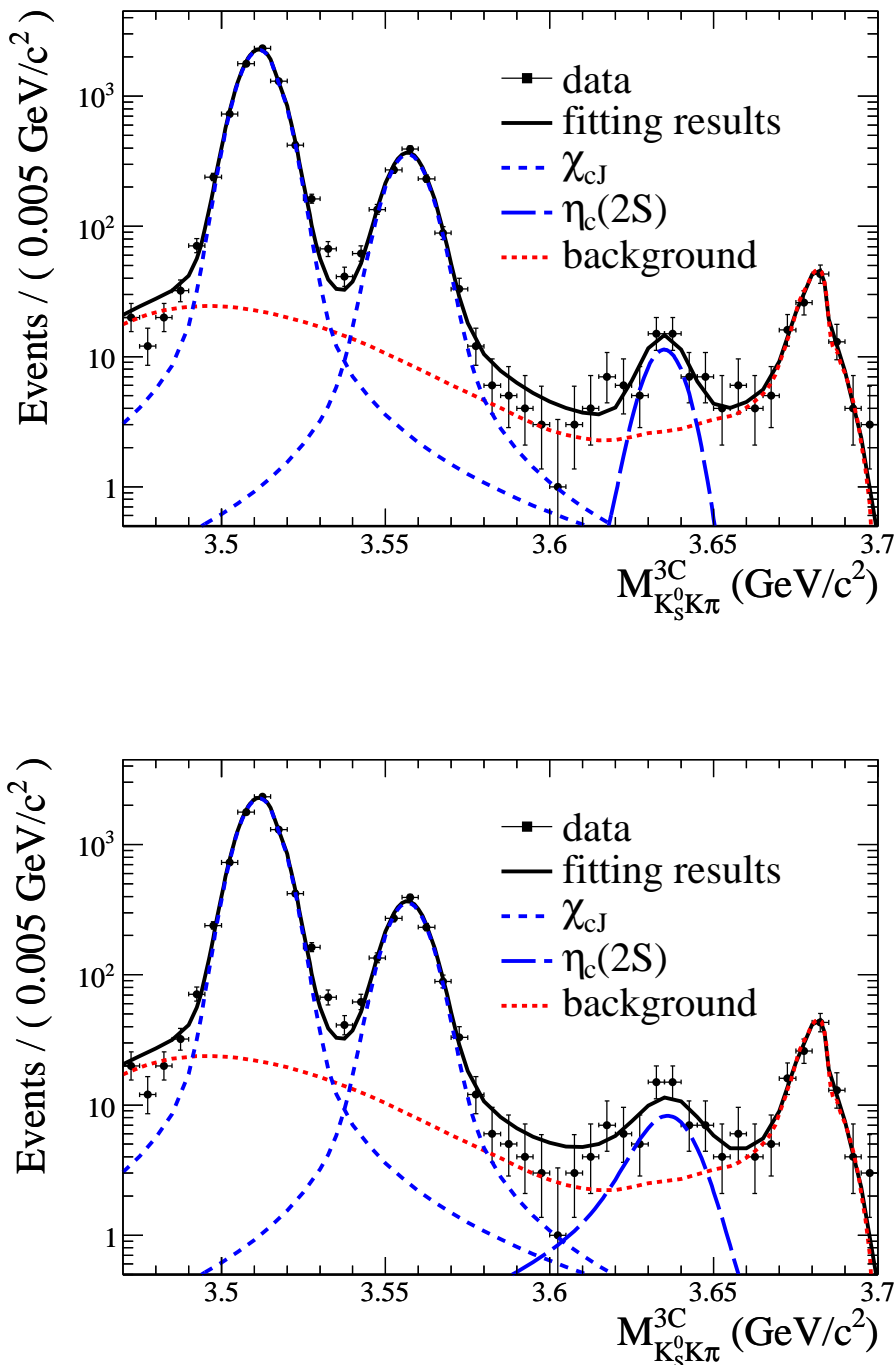


Figure 33: Fitting of the mass spectrum with the $\eta_c(2S)$ width free (top) and fixed (bottom).

Table 5: Results of the mass spectrum fitting

	Fit 1	Fit 2
$M_{\chi_{c1}}$ (MeV/c ²)	3511.460 ± 0.079	3511.460 ± 0.079
$M_{\chi_{c2}}$ (MeV/c ²)	3556.74 ± 0.22	3556.73 ± 0.22
$M_{\eta_c(2S)}$ (MeV/c ²)	3636.8 ± 2.1	3638.6 ± 2.3
$\Gamma_{\eta_c(2S)}$ (MeV/c ²)	3.4 ± 3.5	12 (fixed)
$N_{\eta_c(2S)}$	40 ± 10	47.5 ± 9.4
Statistical significance of $\eta_c(2S)$	6.1σ	6.2σ

Table 6: Summary of χ_{cJ} results.

	N_{obs}	ϵ	$\mathcal{B}(\psi' \rightarrow \gamma\chi_{cJ}, \chi_{cJ} \rightarrow K_S^0 K^\pm \pi^\mp)$	\mathcal{B} from PDG
χ_{c1}	6938 ± 88	27.2%	$(3.48 \pm 0.15) \times 10^{-4}$	$(3.39 \pm 0.34) \times 10^{-4}$
χ_{c2}	1179 ± 37	26.0%	$(6.18 \pm 0.30) \times 10^{-5}$	$(5.81 \pm 0.91) \times 10^{-5}$

48 ± 13 , so the difference between estimation and fitting $\Delta N_{signal} = 15 \pm 14$ is about one standard deviation. If the χ_{c2} MC problem (there is a cut off on the mass up limit) and the mass shift of $K_S^0 K^\pm \pi^\mp$ events are considered, the difference will be even smaller. So they are consist as expected.

- **Check on the branching ratios of χ_{cJ}**

From this analysis, one can also give the measurements of the branching ratios of $\psi' \rightarrow \gamma\chi_{cJ}, \chi_{cJ} \rightarrow K_S^0 K^\pm \pi^\mp$ ($J = 1, 2$). The results from this analysis (only statistic errors included) and the previous results from PDG2010 [5] are summarized in Table 6, which agree with each other rather well for χ_{c1} and χ_{c2} respectively.

- **Check on the selected photons**

The distributions of energy, polar angle, time and $E_{3\times 3}/E_{5\times 5}$ (the energy deposited in the 3*3 crystals around the shower center over the one in the 5*5 crystals) for the selected photons are shown in Figures 34, 35, 36 and 37. For the events in the signal mass region ($3.6 < M_{K_S^0 K^\pm \pi^\mp}^{3C} < 3.66 \text{ GeV}/c^2$), the distributions of the photons for data are quite consistent with real photons (Figure 34). For the events above the signal mass region ($M_{K_S^0 K^\pm \pi^\mp}^{3C} > 3.66 \text{ GeV}/c^2$), most of the selected photons should be fake photons which have different distributions, and the distributions for data are consistent with the background MC (Figure 35). The distributions of the photons in the end-caps have much lower statistics, but still follow the similar behavior (Figure 36 and 37).

8 Results

Though the width can not be well determined by our data (see Fit 1 in Table 5) and is fixed to PDG value, the mass of $\eta_c(2S)$ can be well extracted from the fitting. The systematic errors on the fitted mass are studied and summarized in Table 7. The uncertainty due to mass shift is estimated from the fitted mass for χ_{c1} and χ_{c2} . The background line shape caused uncertainty is evaluated by changing the relative ratio of the $K_S^0 K^\pm \pi^\mp$ background events with radiation over those without radiation. The uncertainty from the form of the damping function on the mass of $\eta_c(2S)$ is estimated to be 0.3 MeV. The error on the fixed width of $\eta_c(2S)$ is 3 MeV, and the effect on the fitted mass is about 0.77 MeV. Others are negligible. So

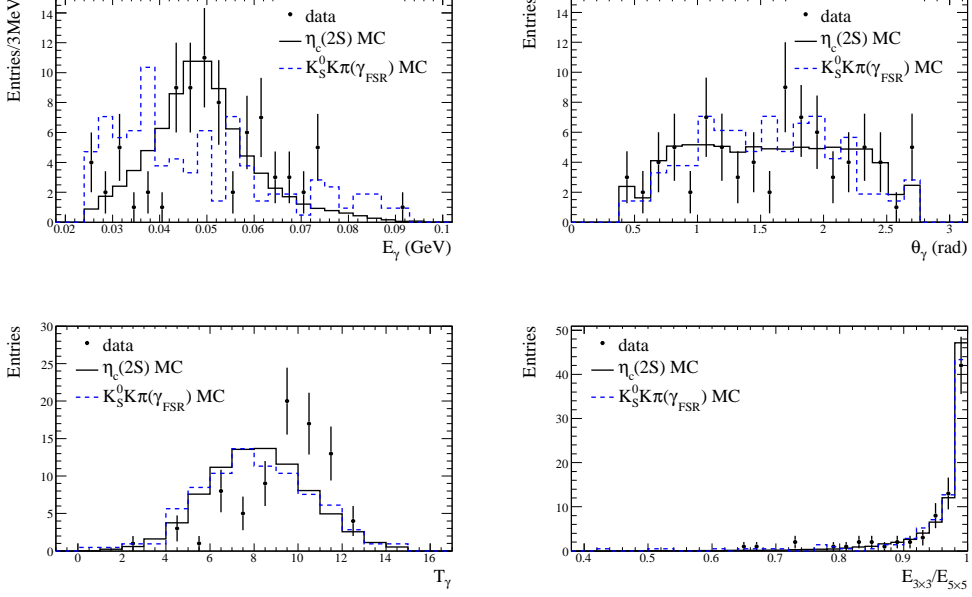


Figure 34: The distributions of the selected photons for the events in the signal mass region ($3.6 < M_{K_S^0 K^\pm \pi^\mp}^{3C} < 3.66 \text{ GeV}/c^2$).

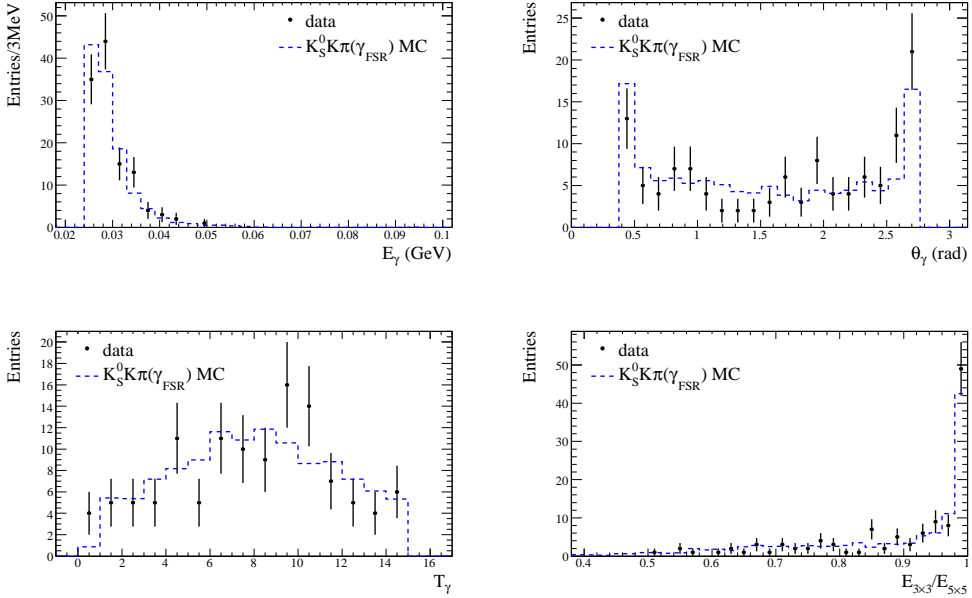


Figure 35: The distributions of the selected photons for the events above the signal mass region ($(M_{K_S^0 K^\pm \pi^\mp}^{3C} > 3.66 \text{ GeV}/c^2)$).

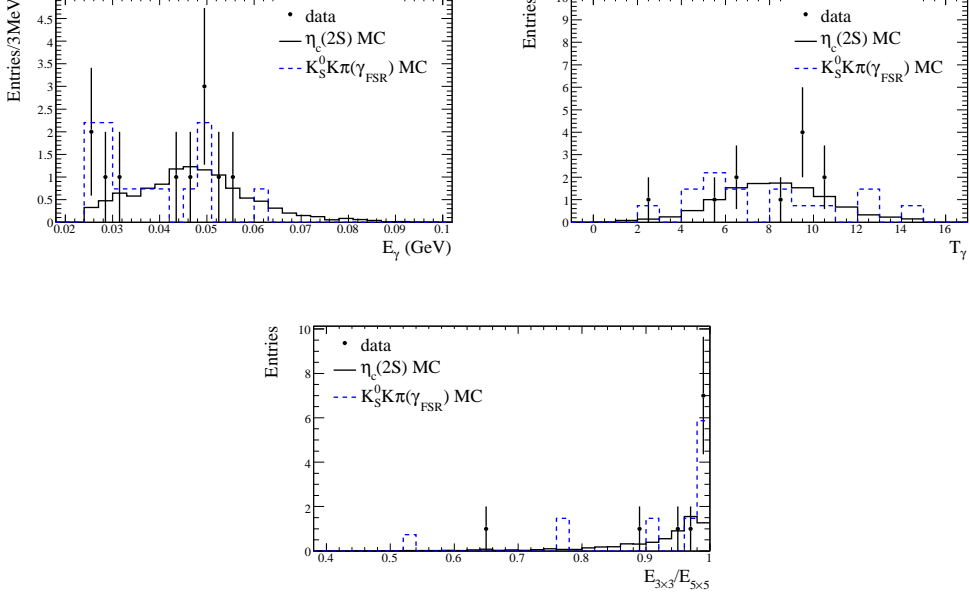


Figure 36: The distributions of the selected photons at end-caps for the events in the signal mass region ($M_{K_S^0 K^\pm \pi^\mp}^{3C} < 3.66 \text{ GeV}/c^2$).

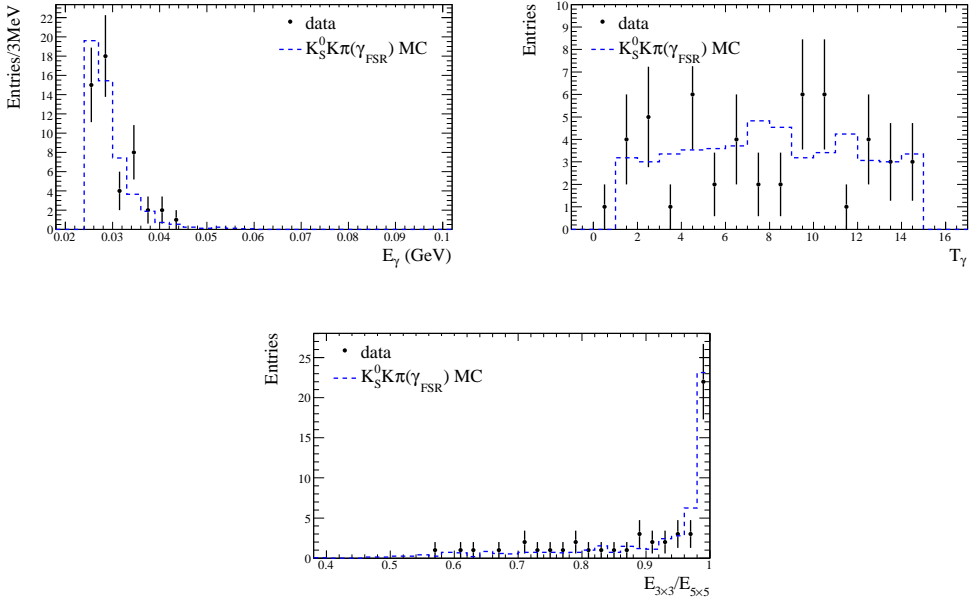


Figure 37: The distributions of the selected photons at end-caps for the events above the signal mass region ($M_{K_S^0 K^\pm \pi^\mp}^{3C} > 3.66 \text{ GeV}/c^2$).

Table 7: The systematic uncertainties on the fitted mass of $\eta_c(2S)$ (in MeV/c²).

source	Systematic uncertainty
mass shift	0.74
BG line shape	0.4
damping function	0.3
width of $\eta_c(2S)$	0.77
mass resolution	0.0
mass range	0.0
total	1.2

the measured mass of $\eta_c(2S)$ is $3638.6 \pm 2.3 \pm 1.2$ MeV/c², where the first error is statistical, the second one is systematic.

From the fitted number of events for the $\eta_c(2S)$ signal, one can obtain the branching ratio for $\psi' \rightarrow \gamma\eta_c(2S), \eta_c(2S) \rightarrow K_S^0 K^\pm \pi^\mp$ as:

$$\begin{aligned} \mathcal{B}(\psi' \rightarrow \gamma\eta_c(2S)) \times \mathcal{B}(\eta_c(2S) \rightarrow K_S^0 K^\pm \pi^\mp) &= \frac{N_{\eta_c(2S)}}{\epsilon \cdot \mathcal{B}(K_S^0 \rightarrow \pi^+ \pi^-) \cdot N_{\psi'}} \\ &= \frac{47.5}{0.2316 \times 0.692 \times (1.06 \times 10^8)} \\ &= (2.80 \pm 0.56) \times 10^{-6}, \end{aligned} \quad (8)$$

where ϵ is the efficiency of the event selection from full simulation, $\mathcal{B}(K_S^0 \rightarrow \pi^+ \pi^-)$ is the branching ratio for $K_S^0 \rightarrow \pi^+ \pi^-$, and $N_{\psi'}$ is the total number of ψ' . Table 8 shows the systematics on the measured branching ratio $\mathcal{B}(\psi' \rightarrow \gamma\eta_c(2S)) \times \mathcal{B}(\eta_c(2S) \rightarrow K_S^0 K^\pm \pi^\mp)$. So the final result of the measured branching ratio is $\mathcal{B}(\psi' \rightarrow \gamma\eta_c(2S)) \times \mathcal{B}(\eta_c(2S) \rightarrow K_S^0 K^\pm \pi^\mp) = (2.80 \pm 0.56 \pm 0.50) \times 10^{-6}$. If the measurement from BaBar $\mathcal{B}(\eta_c(2S) \rightarrow K\bar{K}\pi) = (1.9 \pm 0.4 \pm 1.1)\%$ [20] is taken, together with our measurement, one can derive the M1 transition rate between ψ' and $\eta_c(2S)$:

$$\mathcal{B}(\psi' \rightarrow \gamma\eta_c(2S)) = \frac{2.80 \times 10^{-6}}{1.9\% \times \frac{1}{3}} = (4.4 \pm 0.9 \pm 2.8) \times 10^{-4}, \quad (9)$$

where the systematic error is dominated by the BaBar result.

9 Summary

Using the largest ψ' data sample in the world which was collected by BESIII, we searched for the M1 transition between ψ' and $\eta_c(2S)$ through the hadronic final states $K_S^0 K^\pm \pi^\mp$. Finally, a signal with a statistical significance of 6.2 standard deviation is observed which is the first observation of the M1 transition between ψ' and $\eta_c(2S)$. The measured mass for $\eta_c(2S)$ is $3638.6 \pm 2.3 \pm 1.2$ MeV/c². The measured branching ratio is $\mathcal{B}(\psi' \rightarrow \gamma\eta_c(2S)) \times \mathcal{B}(\eta_c(2S) \rightarrow K_S^0 K^\pm \pi^\mp) = (2.80 \pm 0.56 \pm 0.50) \times 10^{-6}$. Together with the Babar result $\mathcal{B}(\eta_c(2S) \rightarrow K\bar{K}\pi) = (1.9 \pm 0.4 \pm 1.1)\%$, the M1 transition rate between ψ' and $\eta_c(2S)$ is derived as $\mathcal{B}(\psi' \rightarrow \gamma\eta_c(2S)) = (4.4 \pm 0.9 \pm 2.8) \times 10^{-4}$.

Table 8: The systematic errors on the measured branching ratio $\mathcal{B}(\psi' \rightarrow \gamma\eta_c(2S)) \times \mathcal{B}(\eta_c(2S) \rightarrow K_S^0 K^\pm \pi^\mp)$.

Source	Systematics
BG line shape	13%
damping function	7.6%
width of $\eta_c(2S)$	4.8%
tracking	2.5%
K_S^0 reconstruction	3.5%
4-C kinematic fitting (χ^2 cut)	3.6%
photon reconstruction	1%
intermediate states in $\eta_c(2S) \rightarrow K_S^0 K^\pm \pi^\mp$	2.5%
number of ψ'	4%
total	18%

References

- [1] J. J. Aubert *et al.*, Phys. Rev. Lett. 33, 1404 (1974).
- [2] J. E. Augustin *et al.*, Phys. Rev. Lett. 33, 1406 (1974).
- [3] G. S. Abrams *et al.*, Phys. Rev. Lett. 33, 1453 (1974).
- [4] D. Cronin-Hennessy, K. Y. Gao *et al.* (CLEO-_C Collaboration), Phys. Rev. D 81, 052002 (2010). (2008) and 2009 partial update for the 2010 edition.
- [5] K. Nakamura *et al.*, Journal of Physics G 37, 075021 (2010).
- [6] M. Ablikim *et al.* (BESIII Collaboration), Phys. Rev. D 81, 052005 (2010)
- [7] Xu Min *et al.*, Chinese Physics C, 34(1): 92-98 (2010)
- [8] E. Barberio and Z. Was, Comput. Phys. Commun. 79, 291 (1994).
- [9] M. Ablikim *et al.* (BES Collaboration), Phys. Lett. B 614, 37 (2005).
- [10] Ma Tian, talk on the efficiency of K_S^0 reconstruction at the DQ/Validation Meeting on 8th May (2010).
- [11] Zhu Kai, talk "Tracking and PID Efficiency of Pion and Proton" in BESIII Software/Physics Workshop Feb (2010)
- [12] Ye Chen, Jiaxu Zuo, talk at the DQ/Validation Meeting on 18th January (2010)
- [13] M. Ablikim *et al.* (BESIII Collaboration), Phys. Rev. D 81, 052005 (2010).
- [14] Y.Q. WANG, talk "Search for new $\eta_c(2S)$ decays" at the BESIII Collaboration 2010 Fall Meeting.
- [15] V.V. Anashin *et al.*, arXiv:1012.1694 [hep-ex]

- [16] R. E. Mitchell *et al.* (CLEO Collaboration), Phys. Rev. Lett. 102, 011801 (2009).
- [17] N. Brambilla, P. Roig and A. Vairo, arXiv:1012.0773v1 [hep-ph] 3 Dec 2010.
- [18] V. Druzhinin (for BaBar Collaboration), talk "Recent results on two-photon physics at BaBar" at ICHEP 2010.
- [19] H. Nakazawa (for Belle Collaboration), talk "Particle production in two-photon collisions at Belle" at ICHEP 2010.
- [20] B. Aubert *et al.* (Babar Collaboration), Phys. Rev. D 78, 012006 (2008)